Water Resources Research

RESEARCH ARTICLE
10.1029/2023WR035625

Hyporheic Flows in Stratified Sediments: Implications on Residence Time Distributions

Alessandra Marzadri[1], **Valentina Ciriello**[2], **and Felipe P. J. de Barros**[3]

[1]Department of Civil, Environmental and Mechanical Engineering, University of Trento, Trento, Italy, [2]Department of Civil, Chemical, Environmental and Materials Engineering, University of Bologna, Bologna, Italy, [3]Sonny Astani Department of Civil and Environmental Engineering, University of Southern California, Los Angeles, CA, USA

Key Points:

- A new integral transform-based semi-analytical solution for hyporheic flows in stratified sediments is provided and tested against data
- The impact of hydraulic conductivity stratification on residence time distribution and its statistics is quantitatively analyzed
- ROMs are used to approximate key residence time statistics in the space of variability of parameters characterizing the conductivity profile

Correspondence to:
F. P. J. de Barros,
fbarros@usc.edu

Citation:
Marzadri, A., Ciriello, V., & de Barros, F. P. J. (2024). Hyporheic flows in stratified sediments: Implications on residence time distributions. *Water Resources Research*, *60*, e2023WR035625. https://doi.org/10.1029/2023WR035625

Received 20 JUN 2023
Accepted 13 DEC 2023

Author Contributions:
Conceptualization: Alessandra Marzadri, Felipe P. J. de Barros
Formal analysis: Alessandra Marzadri, Valentina Ciriello, Felipe P. J. de Barros
Investigation: Alessandra Marzadri, Valentina Ciriello, Felipe P. J. de Barros
Methodology: Alessandra Marzadri, Valentina Ciriello, Felipe P. J. de Barros
Software: Alessandra Marzadri, Valentina Ciriello, Felipe P. J. de Barros
Validation: Alessandra Marzadri, Valentina Ciriello
Visualization: Alessandra Marzadri, Valentina Ciriello, Felipe P. J. de Barros
Writing – original draft: Alessandra Marzadri, Valentina Ciriello, Felipe P. J. de Barros

Abstract The fate of nutrients and contaminants in fluvial ecosystems is strongly affected by the mixing dynamics between surface water and groundwater within the hyporheic zone, depending on the combination of the sediment's hydraulic heterogeneity and dune morphology. This study examines the effects of hydraulic conductivity stratification on steady-state, two-dimensional, hyporheic flows and solute residence time distribution. First, we derive an integral transform-based semi-analytical solution for the flow field, capable of accounting for the effects of any functional shape of the vertically varying hydraulic conductivity. The solution considers the uneven distribution of pressure at the water-sediment interface (i.e., the pumping process) dictated by the presence of dune morphology. We then simulate solute transport using particle tracking. Our modeling framework is validated against numerical and tracer data from flume experiments and used to explore the implication of hydraulic conductivity stratification on the statistics and *pdf* of the residence time. Finally, reduced-order models are used to enlighten the dependence of key residence time statistics on the parameters characterizing the hydraulic conductivity stratification.

1. Introduction

The exchange of water and solutes across the streambed interface regulates biogeochemical and ecological processes in fluvial systems (Boano et al., 2008; Tonina, 2012). Stream waters downwell into the sediment and exit back into the stream at upwelling zones resulting in what is known as the *hyporheic exchange* (Elliott & Brooks, 1997; Packman et al., 2000; Savant et al., 1987). The hyporheic exchange is one of the key mechanisms driving solute and oxygen-rich stream waters into the sediments, thus generating hydraulic and chemical gradients that sustain an ecosystem (Bencala & Walters, 1983; Findlay, 1995). The hydrodynamics in the hyporheic zone is mainly controlled by two factors: (a) the spatiotemporal dynamics of the near-bed energy heads generated primarily by stream hydro-morphology (i.e., the pumping process) and (b) the spatial heterogeneity of hydraulic conductivity field within the streambed sediment (Nelson et al., 2019; Ryan & Boufadel, 2006; Su et al., 2020).

Many works have proposed models to predict the flow field within the hyporheic zone induced by the morphology of the streambed. For example, Elliott and Brooks (1997) provide a physically based model together with an analytical solution to analyze the effects of dune morphology on the exchange of solutes in a hyporheic zone characterized by a homogeneous bed of infinite thickness. Extensions of the analysis carried out by Elliott and Brooks (1997) for a finite bed thickness are also reported in the literature for dune morphology (Packman et al., 2000), pool-riffle morphology (Marzadri et al., 2010; Tonina & Buffington, 2007) and stream meanders (Boano et al., 2010; Stonedahl et al., 2013). The interaction between the hyporheic and groundwater fluxes can also impact the solute residence time distribution (hereafter RTD). Boano et al. (2008) investigated the effect of groundwater inflow on the reduction of the hyporheic zone volume, whereas Fox et al. (2016) measured the impact of groundwater losing and gaining flow conditions on hyporheic exchange fluxes through laboratory flume experiments. Marzadri et al. (2016) derived an analytical solution for the hydraulic head and the hyporheic flow field under gaining/losing groundwater flow conditions considering homogeneous streambed sediments. All of the above-mentioned works rely on the classic Tóth approach, which replaces the streambed surface topography with a flat surface (Tóth, 1963). The key assumption employed by Tóth (1963) is that the magnitude of the scale of the topographical undulations is much smaller than the vertical scale of the flow domain. The validity of this assumption was rigorously investigated through the use of perturbation theory (Frei et al., 2019).

Compared to previous studies that aimed to examine the effects of pumping, research focused on the role of hydraulic conductivity heterogeneity on hyporheic exchange is limited and often characterized by different

Writing – review & editing: Alessandra Marzadri, Valentina Ciriello, Felipe P. J. de Barros

findings reflecting diverse assumptions and boundary conditions. Often, especially when considering the reach or watershed scales, the effects of streambed heterogeneity are neglected because of a combination of data paucity (crucial to characterize the hydraulic conductivity) and easiness of calculation. Most studies focusing on the impact of conductivity heterogeneity on solute exchange pathways and the RTD rely on the numerical solution of the governing equations (Cardenas et al., 2004; Fox et al., 2016; Hester et al., 2013; Jiang et al., 2020; Salehin et al., 2004; Sawyer & Cardenas, 2009; Su et al., 2020; Tonina et al., 2016; Trauth et al., 2013); thus indicating the complexities associated with the mathematical treatment of flow and transport through heterogeneous porous media. An interesting case occurs when streambed heterogeneity is determined by the morphology evolutionary cycle (i.e., categorical heterogeneity), reflecting in a layered structure of the hyporheic zone dictated by the sedimentary facies architecture (e.g., Buffington & Montgomery, 1999, and reference therein). Within this context, Jiang et al. (2020) utilized numerical simulations to show how a low-permeability layer in a stratified streambed impacts the vertical spreading of a solute plume. Analytical solutions can be derived depending on the conceptualization of sediment heterogeneity. For example, Marion et al. (2008) proposed an analytical solution for the hyporheic flow in a two-layer streambed under the Tóth assumption and they imposed the continuity of the hydraulic head at the interface of both layers without considering the continuity of the flux condition.

In this work, we derive a computationally efficient modeling framework (validated against numerical and experimental data) to study how the stratified structure of the streambed hydraulic conductivity impacts the flow field and the solute RTD within the hyporheic zone. Different than previous works, we derive a semi-analytical expression for the spatially variable flow field within the hyporheic zone. We conceptualize the heterogeneous structure of the hyporheic zone through a *single-domain mathematical formulation*. In other words, one can represent the fluctuations of the hydraulic properties of the medium through spatially variable coefficients in the governing flow equation (e.g., de Barros & Cotta, 2007; de Barros et al., 2006). This avoids the need to couple the solutions of the flow equation at different layers with interface boundary conditions. The derived solution is based on integral transforms (Cotta, 1993; Mikhailov & Ozisik, 1994) and takes into account any functional shape of the vertically varying hydraulic conductivity. To exemplify our approach, we adopt a four-parameter logistic-type function to mimic the hydraulic conductivity vertical profile. We observe that by varying the parameters of this logistic-type function, we can reproduce a wide range of stratified structures, including the sand and gravel alluvial formations observable in the field. Subsequently, we combine the semi-analytical flow solution with particle tracking simulations to investigate how the conductivity contrasts in a two-layered and a three-layered formation impact the statistics and the probability density function (hereafter *pdf*) of the residence time. Finally, we construct reduced-order models (hereafter ROMs) to express the variability of key residence time statistics in terms of the parameters of the logistic-type function characterizing the conductivity profile. We employ a class of ROMs, namely the Polynomial Chaos Expansion (hereafter PCE) (Ghanem & Spanos, 1991; Xiu & Karniadakis, 2002), which has been used for uncertainty quantifications and global sensitivity analysis under different hydrological settings and applications (e.g., Ciriello & de Barros, 2020; Ciriello et al., 2017, 2019; Oladyshkin et al., 2012).

The paper is organized as follows: in Section 2, the problem formulation is presented, while Section 3 is devoted to the derivation of the novel semi-analytical solution of the hyporheic flow field and the use of particle tracking to characterize solute transport in terms of residence time, Section 4 is dedicated to the application of the proposed model to investigate the implications of the conductivity contrasts in a two-layered and a three-layered formation on the RTD and Section 5 is devoted to the use of the ROMs to fully characterize the dependence of key residence time statistics on the parameters defining the conductivity profile. Finally, Section 6 provides a summary of the results.

2. Physical Formulation

The problem formulation consists of the mathematical description of the flow field within the hyporheic zone and the transport problem. We start by considering a steady-state two-dimensional (2-D) flow field within a spatially heterogeneous streambed where the Cartesian coordinate system is given by $\mathbf{x} = (x, z)$ (see Figure 1). Heterogeneity stems from the vertical variability of the hydraulic conductivity $K \equiv K(z)$. In our work, we follow the approach proposed by Tóth (1963) and Packman et al. (2000), where the hyporheic flow is induced by dune-like bedforms

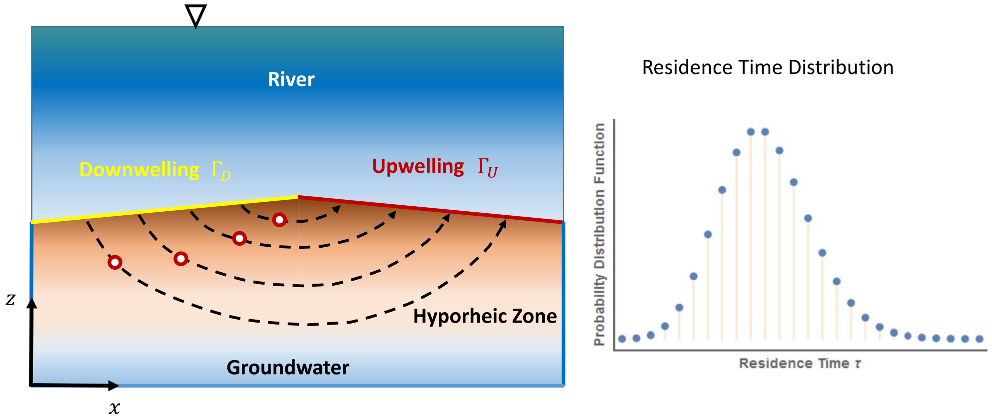

Figure 1. Schematic illustration of the problem analyzed. Solute particles enter the hyporheic zone through the downwelling zone (Γ_D) and exit through the upwelling zone (Γ_U). The shape of the *pdf* of the residence time of each solute particle within the hyporheic zone (residence time distribution) will depend on the spatial patterns of the hydraulic conductivity characterizing the sediment.

in the rectangular domain Ω. The flow domain is a 2-D rectangle given by $\Omega = \{(x, z) | x \in [0, L], z \in [0, d_b]\}$, with L the dune length and d_b the hyporheic zone thickness. The governing flow equation is:

$$K(z)\frac{\partial^2 h(x,z)}{\partial x^2} + \frac{\partial}{\partial z}\left[K(z)\frac{\partial h(x,z)}{\partial z}\right] = 0, \tag{1}$$

with h denoting the hydraulic head. The variability of the hydraulic conductivity is automatically taken into consideration by allowing the coefficients of the partial differential Equation 1 to vary in space in a single domain formulation. Similar single domain modeling strategies were adopted in the past to simulate transport phenomena in rivers and channels with spatial fluctuations in both velocity and eddy diffusivities due to the presence of obstructions (i.e., vegetation) and boundary effects (e.g., de Barros & Cotta, 2007; de Barros et al., 2006; Rubol et al., 2016). Other approaches consist of solving the flow equation in multiple layers of uniform conductivity and coupling the solution through boundary conditions at the interface between these layers. To obtain the 2-D flow field, Equation 1 is solved by considering that the stream water discharge is constant or slowly varying over time preventing the turnover phenomena (i.e., the dune migration), thus allowing us to employ the steady-state assumption. Transient effects can be considered by considering a succession of steady states for the hydraulic head (i.e., quasi-steady-state). The proposed solution also considers a 2-D domain. The 2-D assumption is in agreement with typical conditions used to model natural streambeds characterized by dunes (Elliott & Brooks, 1997; Hester et al., 2013; Packman et al., 2000). For other types of streambed morphology (i.e. pool-riffles, meanders, etc.), 3-D representations of the hyporheic flow is more suitable both under homogeneous (Marzadri et al., 2010; Tonina & Buffington, 2007) and heterogeneous (Boano et al., 2010; Trauth et al., 2013; Zijl, 1999) conditions.

Equation 1 is subject to the following set of boundary conditions along the longitudinal and vertical directions:

$$\left.\frac{\partial h(x,z)}{\partial x}\right|_{x=0} = -s, \qquad \left.\frac{\partial h(x,z)}{\partial x}\right|_{x=L} = -s \tag{2}$$

and

$$h(x, d_b) = f(x), \qquad \left.\frac{\partial h(x,z)}{\partial z}\right|_{z=0} = \pm\frac{q_g}{K_g}, \tag{3}$$

where q_g represents the groundwater-specific discharge, K_g corresponds to the hydraulic conductivity of the underlying aquifer, and s is the stream slope. Note that the "+" and "−" signs in the second boundary condition given in Equation 3 indicate a gaining and losing conditions. Without loss of generality, we consider the following functional form for $f(x)$ (Marzadri et al., 2016):

$$f(x) = h_m \cos(\lambda x) - s\,x \tag{4}$$

where $\lambda = 2\pi/L$ is the dune wave number and h_m is the amplitude of the hydraulic head distribution at the streambed interface. In our work, we compute h_m as (Shen et al., 1990):

$$h_m = \frac{0.28V^2}{2g}\begin{cases}\left(\frac{H_d/Y_0}{0.34}\right)^{3/8} & \text{if } H_d/Y_0 \leq 0.34\\ \left(\frac{H_d/Y_0}{0.34}\right)^{3/2} & \text{if } H_d/Y_0 > 0.34\end{cases} \tag{5}$$

where Y_0 is the mean flow depth, H_d is the dune height, V is the mean velocity in the stream, and g is the gravitational acceleration. Solving Equation 1 under the boundary conditions and functional relationships provided in Equations 2–5, we obtain the distribution of $h(x, z)$ which allows for the evaluation of the velocity field $\mathbf{u} = (u, w)$ within the hyporheic zone through the use of the Darcy's law:

$$\mathbf{u}(\mathbf{x}) = -\frac{K(z)}{\phi}\nabla h(\mathbf{x}) \tag{6}$$

where ϕ is the porosity of the sediment (assumed to be constant) and $\mathbf{u} = (u, w)$ is the velocity field vector.

Here, to mimic the hydraulic conductivity profile of a broad range of stratified structures of the streambed, the following four-parameter logistic-type function is used:

$$K(z) = K_g + \sum_{i=1}^{N_K} \frac{\alpha^{(i)}}{1 + \exp\left[-\frac{1}{k_r^{(i)}}\left(\frac{z}{d_b} - \gamma_t^{(i)}\right)\right]}, \tag{7}$$

where the parameter α is an amplification factor that takes into account the increment ($\alpha > 0$) or the decrement ($\alpha < 0$) of the hydraulic conductivity value with respect to K_g. The parameter k_r defines how smoothly the variation in the hydraulic conductivity between two successive strata (i.e., the higher is k_r, more abrupt the change in the hydraulic conductivity profile). Finally, γ_t represents a representative dimensionless depth at which the change in K occurs (i.e., between two successive strata). The summation in Equation 7 is employed to represent the number ($i = 1,\ldots,N_K$) of layers in the sediment. Figure 2 illustrates the flexibility of Equation 7 to adopt different number of layers and the smoothness of the transition between the conductivity values.

According to previous findings (Cardenas et al., 2008; Marzadri et al., 2012), transport of a passive tracer in the hyporheic zone is assumed to be purely advective and governed by the following differential equation:

$$\frac{\partial C(x,z,t)}{\partial t} + u(x,z)\frac{\partial C(x,z,t)}{\partial x} + w(x,z)\frac{\partial C(x,z,t)}{\partial z} = 0. \tag{8}$$

We consider Dirichlet boundary conditions at the downwelling (Γ_D) region, see Figure 1. The concentration of the dissolved solute in the river is C_0 such that $C(x, z, t) = C_0$ for $(x, z) \in \Gamma_D \cup \Gamma_U$. As for the initial condition, we assume that at $t = 0$ the tracer concentration within the hyporheic zone is zero, that is, $C(x, z, 0) = 0$. Due to the purely advective process and $\nabla \cdot \mathbf{u} = 0$, a family of characteristics for Equation 8 can be obtained, namely, $\dot{\mathbf{x}}(t) = \mathbf{u}(\mathbf{x})$ with $\mathbf{x}(0) = \mathbf{x}_d$ for $\mathbf{x}_d \in \Gamma_D$.

3. Solution

This section describes the solution of flow and transport in the hyporheic zone according to the proposed modeling framework. A comparison of our findings with numerical and experimental data is provided in Appendix A.

3.1. Semi-Analytical Solution for the Flow Field

We use the Generalized Integral Transform Technique (GITT) (Cotta, 1993) to solve the elliptic PDE (Equation 1), subject to the boundary conditions (2) and (3). The GITT is a hybrid numerical-analytical methodology that borrows its principles from the classical integral transform method (Mikhailov & Ozisik, 1994). Its application to elliptic problems is well documented in the fluid flow and heat transfer communities (e.g., Barbuto & Cotta, 1997; Knupp et al., 2015). The GITT has also been employed to compute scalar distributions in a variety

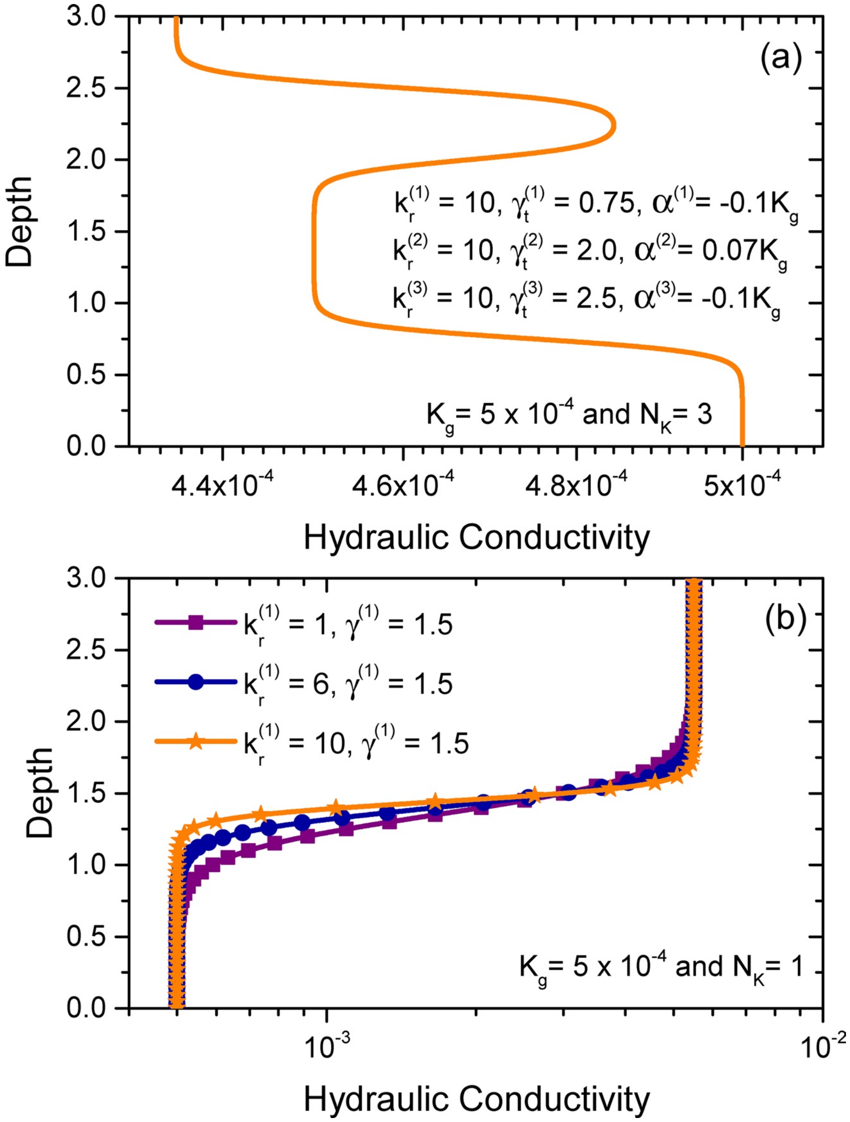

Figure 2. Illustration of the vertical hydraulic conductivity profiles and the flexibility of Equation 7 to capture different, multi-modal, profiles: (a) multi-modal conductivity profile and (b) two-layer conductivity structure. Here, we keep the units generic for the purpose of illustration, for example, depth [L] and hydraulic conductivity [L/T].

of environmental flows such as the ones occurring in fluvial systems and porous-fractured media (e.g., Bonazzi et al., 2021; Cotta et al., 2020; de Barros & Cotta, 2007; Ling et al., 2021; Rubol et al., 2016).

Following Mikhailov and Ozisik (1994) and Cotta (1993), we start by proposing the following integral transform pair:

$$\widehat{h}_i(z) = \int_0^L h(x,z)\psi_i(x)dx \tag{9}$$

$$h(x,z) = \sum_{i=0}^{\infty} \frac{1}{\mathcal{N}_i}\widehat{h}_i(z)\psi_i(x) \tag{10}$$

where $\psi_i(x)$ are the eigenfunctions associated with the ith eigenvalue. The norm $\mathcal{N}_i$ is defined as:

$$\mathcal{N}_i = \int_0^L \psi_i(x)^2 dx. \tag{11}$$

The associated eigenvalue problem which provides the basis for the expansion of the hydraulic head h is given by:

$$\frac{d^2\psi_i(x)}{dx^2} + \beta_i^2\psi_i(x) = 0 \tag{12}$$

$$\left.\frac{d\psi_i(x)}{dx}\right|_{x=0} = 0 \quad \left.\frac{d\psi_i(x)}{dx}\right|_{x=L} = 0 \tag{13}$$

Solving Equations 12 and 13, we obtain $\psi_i(x) = \cos(\beta_i x)$ where the eigenvalues are $\beta_i = i\pi/L$ for $i = 0, 1, 2, \ldots, \infty$. Therefore, the norm $\mathcal{N}_i$ becomes:

$$\mathcal{N}_i = \begin{cases} \frac{L}{2} & \text{for } \beta_i \neq 0 \\ L & \text{for } \beta_i = 0. \end{cases} \tag{14}$$

Multiplying Equation 1 by the eigenfunction ψ_i and integrating along x, we obtain the following expression:

$$\int_0^L \psi_i(x)K(z)\frac{\partial^2 h(x,z)}{\partial x^2}dx + \int_0^L \psi_i(x)\frac{\partial}{\partial z}\left[K(z)\frac{\partial h(x,z)}{\partial z}\right]dx = 0. \tag{15}$$

Integration by parts, together with the eigenvalue problem (Equation 12), yields the following system of ordinary differential equations:

$$\frac{\partial}{\partial z}\left[K(z)\frac{\partial \hat{h}_i(z)}{\partial z}\right] - \beta_i^2 K(z)\hat{h}_i(z) = -Ks[\psi_i(0) - \psi_i(L)] \tag{16}$$

subject to:

$$\hat{h}_i(0) = \hat{f}_i, \quad \text{and} \quad \left.\frac{d\hat{h}_i(z)}{dz}\right|_{z=0} = \pm\hat{Q}_i \tag{17}$$

where $\hat{f}_i$ and $\hat{Q}_i$ are the transformed boundary conditions:

$$\hat{Q}_i \equiv \int_0^L \frac{q_g}{K_g}\psi_i(x)dx; \tag{18}$$

$$\hat{f}_i \equiv \int_0^L f(x)\psi_i(x)dx, \tag{19}$$

where the function $f(x)$ is given in Equation 4. However, other functional shapes for $f(x)$, besides the one provided in Equation 4, can be adopted (Marklund & Wörman, 2011; Nikora et al., 1997; Stonedahl et al., 2010; Wörman et al., 2007).

Note that Equations 16 and 17 form an infinite system of non-homogeneous coupled ordinary differential equations with variable coefficients. Given the variability of the hydraulic conductivity, Equations 16 and 17 are solved numerically in order to obtain $\hat{h}_i(z)$. However, only a truncated version of this system can be solved, that is, $i = 0, 1, \ldots, S_{\max}$ where $S_{\max}$ is the truncation order. The truncation order $S_{\max}$ is determined through a convergence analysis, that is, $S_{\max}$ is defined as soon as the series solution has converged to a desired user-prescribed accuracy. For our work, we solved the truncated system of ordinary differential equations with Mathematica's built-in function `NDSolve`. This built-in function is capable of automatically detecting the best method based on the stiffness of the differential equations. Once the solution is obtained for the transformed hydraulic heads, we invoke the inverse formula, Equation 10, to reconstruct the hydraulic head field $h(x, z)$ for a given truncation order in the eigenfunction expansion. The Darcy scale velocity components can be obtained by substituting Equation 10 into Equation 6:

$$u(x,z) = -\frac{K(z)}{\phi}\sum_{i=0}^{\infty}\frac{\hat{h}_i(z)}{\mathcal{N}_i}\frac{\partial\psi_i(x)}{\partial x} \tag{20}$$

which can be simplified to:

$$u(x,z) = \frac{K(z)}{\phi} \sum_{i=0}^{\infty} \frac{\beta_i}{\mathcal{N}_i} \widehat{h}_i(z) \sin(\beta_i x). \tag{21}$$

The vertical velocity component is obtained as:

$$w(x,z) = -\frac{K(z)}{\phi} \sum_{i=0}^{\infty} \frac{\cos(\beta_i x)}{\mathcal{N}_i} \frac{\partial \widehat{h}_i(z)}{\partial z}, \tag{22}$$

where $\widehat{h}_i$ is the solution of Equations 16 and 17. Given the conductivity profile (Equation 7), u and w can be efficiently computed.

3.2. Particle Tracking for Solute Transport

To simulate transport, we use the particle tracking technique by considering that the mass flux of solute entering the hyporheic zone can be decomposed into a large number of particles, which move under the influence of the velocity field. In the absence of local-scale dispersion and neglecting the effects associated with molecular diffusion, the particle trajectory can be approximated as:

$$\mathbf{X}(t+\Delta t) = \mathbf{X}(t) + \mathbf{u}(\mathbf{X}(t))\Delta t \tag{23}$$

where $\mathbf{X}(t)$ is the particle displacement vector at a given time t and Δt is the simulation time step.

Among the several packages for particle tracking available in the literature (see, e.g., the open-source GPU-based random walk particle tracking code reported in Rizzo et al. (2019)), here, we opt to use the FloPy Python package MODPATH (Bakker et al., 2016; Pollock, 2012). Particle tracking is achieved by post-processing the velocities generated by the semi-analytical solution. Forward particle tracking (i.e., from downwelling to upwelling) is employed by releasing a large number of particles, $N_P = 500$, uniformly distributed along the downwelling area. These particles are then collected at the upwelling area and the residence time of each pathline is computed. The solute residence time is determined by knowing that the mass flux of nonreactive solutes exiting a control volume (resulting from a pulse injection of unitary mass) coincides with the *pdf* of the residence (travel) time of the particles within that control volume (Dagan et al., 1992; Jury et al., 1986). The residence time *pdf* is denoted in our work by g_τ. In our case, the control volume is the hyporheic zone and the exit and entrance surfaces are the upwelling and downwelling areas, respectively. The concentration breakthrough curve at the upwelling area can be written by means of the convolution integral (Małoszewski & Zuber, 1982):

$$C(\tau) = \int_0^{\tau} C_0(\mathbf{x},\tau') g_\tau(\tau') d\tau' \tag{24}$$

where C_0 is the in-stream concentration of solute entering through the downwelling area assumed to be constant (i.e., the solute is well mixed in the stream). Therefore, Equation 24 simplifies to:

$$\frac{C(\tau)}{C_0} = \int_0^{\tau} g_\tau(\tau')\, d\tau' \equiv G_\tau(\tau) \tag{25}$$

where G_τ is the Cumulative Density Function (hereafter *cdf*) of the particle residence time. Thus, the *pdf* of the residence time embeds the dynamics controlling the transport of nonreactive solutes in the hyporheic zone. Accordingly, the residence time *cdf* can be approximated as (Elliott & Brooks, 1997):

$$G_\tau(t) \simeq \frac{\int_{A_{dw}} q(\mathbf{x},0) I(\mathbf{x_d},t)\, d\mathbf{x}}{\int_{A_{dw}} q(\mathbf{x},0)\, d\mathbf{x}} \tag{26}$$

where A_{dw} is the downwelling area through which particles enter the hyporheic zone (see Γ_D in Figure 1). Here, I represents a binary variable: $I = 1$ if the particle released in the downwelling location $\mathbf{x_d} \in \Gamma_D$ at time $t = 0$ is still within the control volume at the time t since its injection, and $I = 0$, if the particle exits the control volume through the upwelling surface at an earlier time. Expression (26) converges to the *cdf* of the residence time as the number of particles increases and the mass carried by a single particle tends to 0.

By considering a pulse of solute that enters the streambed within a small time step ($d\tau$) and remains in it for a certain period of time ($t - \tau$), is possible to obtain: (a) the fraction of mass stored within the sediments at time t (which is proportional to spatially averaged residence time function $\bar{R}$) and (b) the mass accumulated within the sediment per unit of planar bed area with the passing of residence time (τ). The accumulated mass is given by

$$m(t) = \bar{q} \int_0^t \bar{R}(\tau) \frac{C(t-\tau)}{C_0}\, d\tau \tag{27}$$

where $\bar{q}$ is the average flux across the water-sediment interface per stream unit distance. From a dimensional perspective, $m(t)$ can be viewed as the penetration depth at which solutes mixes within the sediments (Elliott & Brooks, 1997).

4. Application and Discussion

Here, we perform a series of simulations to better understand the role of alluvial stratification on *RTD*. In particular, we examine two possible sediment stratification scenarios within the hyporheic zone: (a) a case of a two-layered porous formation and (b) a case of three-layered porous media. The two-layered system is characterized by different hydraulic conductivity and we measure the conductivity contrast by the ratio $\eta = K_2/K_1$ between the upper and the lower one. The three-layered system is composed of an upper and a lower layer characterized by the same hydraulic conductivity (K_1). The middle layer is characterized by a low hydraulic conductivity value, namely K_2. Similar to the two-layered system, we measure the conductivity contrast by the ratio $\eta = K_2/K_1$ between the K of the low conductivity layer and that of the two layers surrounding it. The range of parameters adopted to mimic this behavior is in line with those reported in the literature (Jiang et al., 2020), that is, $K = 6.6 \times 10^{-4}$ to 5.5×10^{-3} m/s, and partially referred to streambed cores collected from the Huaihe River (Anhui Province, China). Other parameters regarding stream hydraulic conditions and dune morphology are selected according to both field (Cisneros et al., 2020) and laboratory studies (Elliott & Brooks, 1997; Marion et al., 2008).

In both stratified scenarios, the model set-up uses the same hydro-morphological parameters of "experiment number 4" reported in Marion et al. (2008) (i.e., the same h_m) but examines the hyporheic flow field in an alluvial streambed with a total depth $d_b = 0.25$ m to consider all the possible hyporheic trajectories. Furthermore, we investigate different scenarios of layer depth, as depicted in Figures 3 and 4 for two-strata and three-strata, respectively. The two-layer system analyzes the following cases: (a) $d_{b1}(=0.2\text{ m}) > d_{b2}(=0.05\text{ m})$, (b) $d_{b1} = d_{b2}(=0.125\text{ m})$, and (c) $d_{b1}(=0.05\text{ m}) < d_{b2}(=0.20\text{ m})$; while the three-layer system consider a lower permeability layer of constant depth $d_l = 0.05$ m located between: (a) $d_{b1}(=0.15\text{ m}) > d_{b2}(=0.05\text{ m})$, (b) $d_{b1} = d_{b2}(=0.10\text{ m})$, and (c) $d_{b1}(=0.05\text{ m}) < d_{b2}(=0.15\text{ m})$. In Figures 3 and 4, the left panels show the vertical variation of the hydraulic conductivity profile, the middle panels display the hydraulic head obtained solving Equation 1, and the right panels present the pathlines connecting downwelling and upwelling areas with arrows every 4.8 hr (based on the solution of Equation 6), for the case $K_1 = 110$ m/d and $K_2 = 44$ m/d (i.e., $\eta = 0.4$). Looking at the six different flow fields in Figures 3 and 4, we can clearly observe the impact of the layer structure in controlling the flow and transport in the hyporheic zone. In particular, the comparison between Figures 3 and 4 underlines the impact of the low permeability layer in confining the flow field near the water-sediment interface; stressing the importance of the strata characteristics and location in controlling the residence time across the streambed sediments. The characterization of the residence time of a water parcel is of significant importance to predict the fate and transport of passive (i.e., temperature) and reactive (i.e., dissolved oxygen, dissolved inorganic nitrogen species, etc.) solutes within the hyporheic zone.

4.1. Implications on Residence Time Statistics

First, we analyze how η affects: the median and the mean hyporeic residence time, τ_{50} and τ_{ave}, respectively; the difference between the 95th and the 5th percentiles, $\tau_{95} - \tau_5$, as a measure of dispersion; the residence time variance, σ^2; the coefficient of variation, CV; and the slope, β, of the descending branch of the RTD (i.e., the tails of the *pdf* calculated near τ_{80}). Figure 5 shows the results of this analysis for the three-layer structure where K_1 is kept constant and equal to 110 m/d; while K_2 is varied between 11 m/d and 99 m/d (i.e., $\eta = 0.1 \div 0.9$).

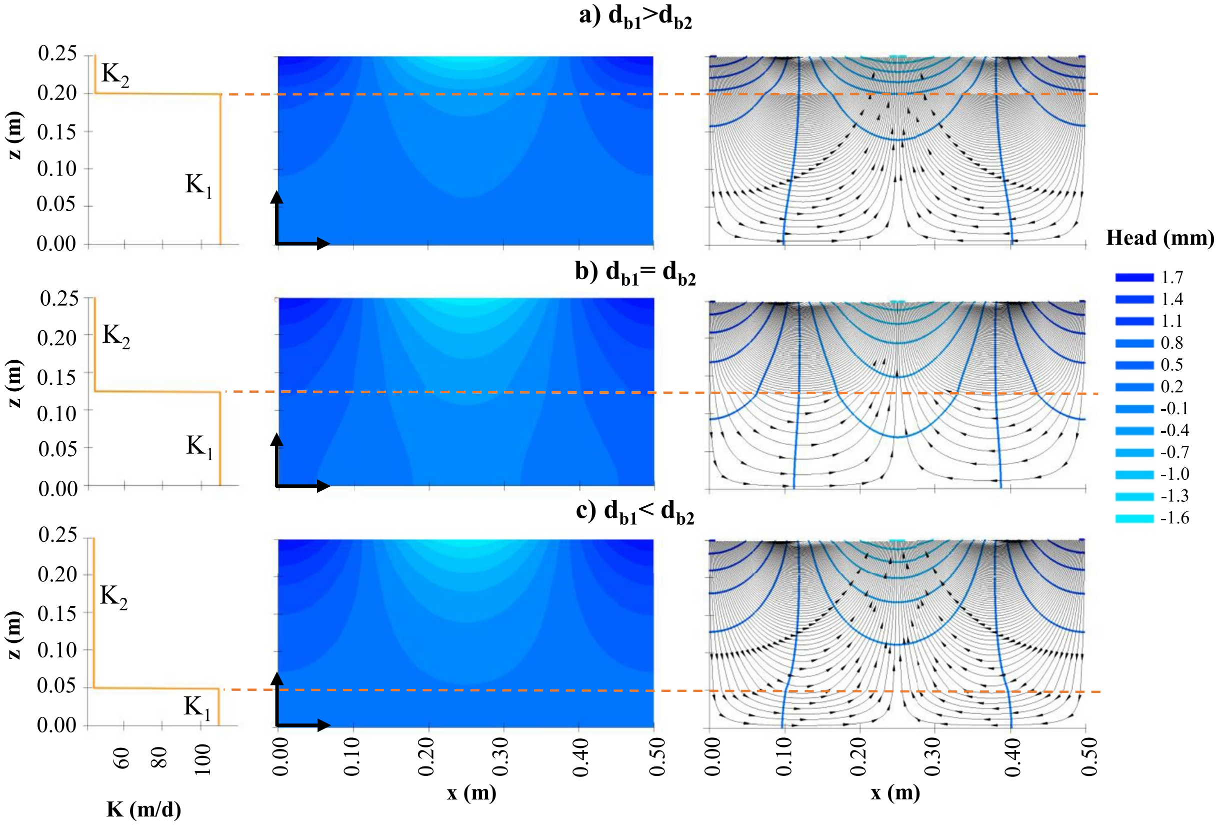

Figure 3. Illustration of the model domain representing the three different scenarios considered to represent the two-layered structure of the hyporheic zone: (a) $d_{b1} > d_{b2}$, (b) $d_{b1} = d_{b2}$, and (c) $d_{b1} < d_{b2}$. For each scenario, the hydraulic conductivity profile (left panel), the hydraulic head (middle panel), and the pathlines (right panel) are shown for $K_1 = 110$ m/d and $K_2 = 44$ m/d (i.e., $\eta = 0.4$).

The variability range in K_2 is selected in order to explore the impact of a lower conductivity layer, located at different depths, on the statistical parameters characterizing the RTD. Similar analysis for the two-layer system reported in Figure 3 is moved, for completeness, to section Appendix C. Note that for the three-layer system, we analyzed only the situation in which the intermediate layer is characterized by low permeability since considering an intermediate layer characterized by high permeability does not produce significant changes in the RTDs.

In Figure 5a, we observe that τ_{50} increases with η for all the different layered structures explored. As shown in Figure 5a, τ_{50} grows at a rate that is inversely proportional to the position of the low permeability layer with respect to the water-sediment interface (i.e., the lower the depth, we observe a higher increase of τ_{50} with η). The results illustrate that even if the hydraulic conductivity layer near the water-sediment interface favors fast transport across the hyporheic zone, the presence of a low conductive layer confines the pathlines, thus preventing the penetration of solute at higher depths. Obviously, this effect fades as η approaches 1. Indeed, for $\eta \sim 1$, the effect of the layer depth on all the statistical parameters is negligible. This is more evident in Figure 5b, where τ_{ave} is higher if the low conductivity layer is located near the water-sediment interface since its presence confines most of the pathlines while at the same time slowing the solute parcels to cross it. This also explains the trends of $\tau_{95} - \tau_5$ and σ^2 in Figures 5c and 5e, respectively. The results in Figures 5c and 5e show a larger variability in the travel times along the single pathlines connecting downwelling and upwelling zones as the location of the low permeability layer moves deep in the streambed (i.e., moving from blue to yellow symbols). Accordingly, the β behavior also reflects this, especially for low values of η (Figure 5d); while as $\eta > 0.4$, the slope of the *pdf* of the RTD appears to be less affected by the position of the low permeability layer. Finally, the coefficient of variation *CV* (Figure 5f) combines the pattern observed in the middle column between $\sqrt{\sigma^2}/\tau_{ave}$. The effect of stratification is extremely important in shaping the *pdf* of the RTD and its parameters, as inferred by comparing the results of Figures 5 and C1 for the three-layer and two-layer

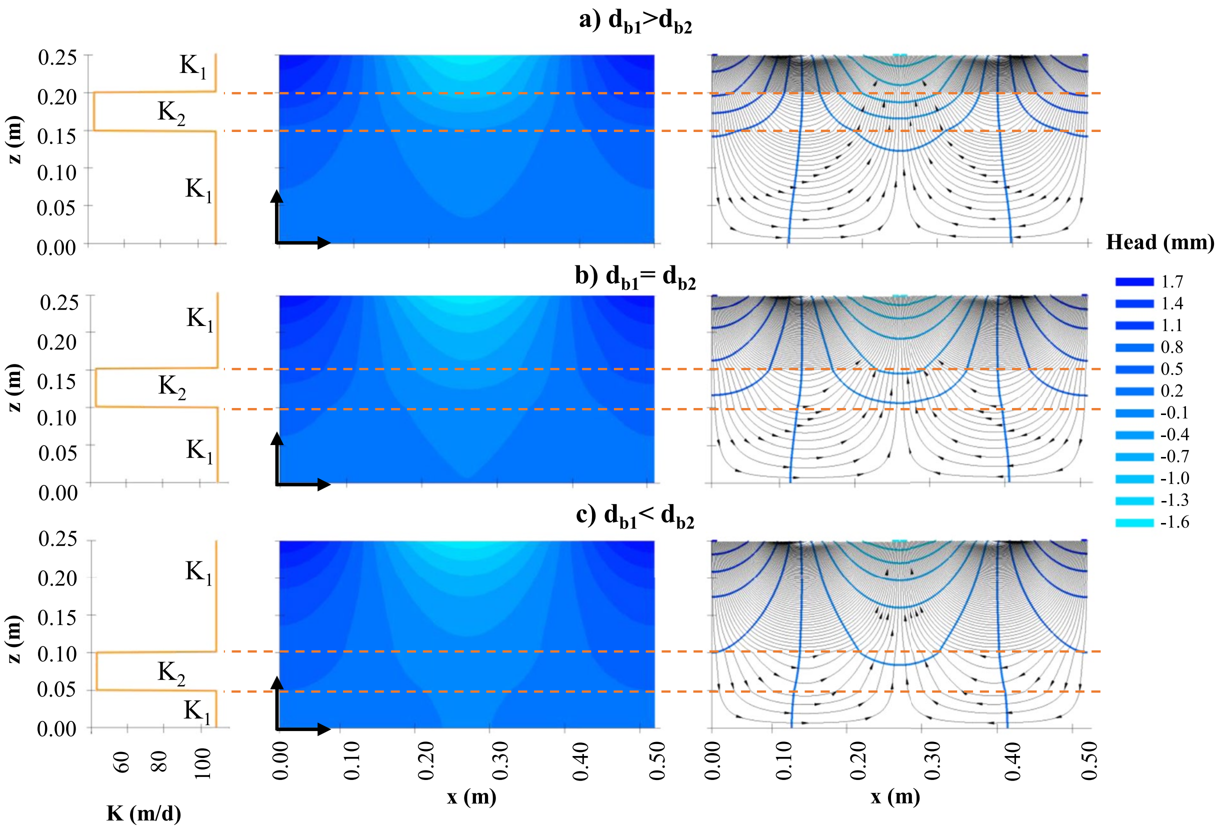

Figure 4. Illustration of the computational domain representing a three-layer system with an upper and a lower layer with higher hydraulic conductivity ($K_1 = 110$ m/d) connected by a low conductivity layer ($K_2 = 44$ m/d) with constant depth of 5 cm. Three different scenarios represent the layered structure of the hyporheic zone: (a) $d_{b1} > d_{b2}$, (b) $d_{b1} = d_{b2}$, and (c) $d_{b1} < d_{b2}$. For each scenario, the hydraulic conductivity profile (left panel), the hydraulic head (middle panel), and the pathlines (right panel) are shown for $\eta = K_2/K_1 = 0.4$.

structures. While in the former is the location of the low permeability layer to shape the RTD, in the latter is the contrast between the hydraulic conductivities. Both layered configurations can represent typical conditions of hyporheic sediments.

Here, we represent the RTD for each layered structure and different η (Figure 6) and vice versa (Figure 7) for the two-layer structure (top row) and the three-layer structure (bottom row), respectively. This analysis embeds most of the observations regarding the behavior of the single residence time statistics presented in the previous section. For example, in Figures 6a and 6b, it is possible to observe the abrupt change in the slope of the RTDs near τ_{80} for $\eta > 1$, thus supporting the behavior of β and CV denoted in Appendix C. Accordingly, in Figure 6d, we can observe the change in the *pdf* slope (compare the curves with orange tones with blue ones) supporting the trend of variation of β in Figure 5d. The effect of stratification is clearly underlined by comparing the top and bottom panels of Figure 6. As shown in Figure 6, an abrupt change in hydraulic conductivity (induced by the presence of a low permeability layer) compacts the flow field and reduces the residence time along the hyporheic pathlines.

In Figure 7, RTDs for two- (top row) and three- (bottom row) layered structures are depicted for selected values of $\eta < 1$. As expected, for higher values of η (Figures 7c–7f), the RTD is less influenced by the thickness of the layered structure; while for lower values of η (Figures 7a, 7b, 7d, and 7e), we can observe the interplay of the conductivity contrast and the depths of the strata. In the two-layer system (Figures 7a and 7b), this results in a two-peak *pdf*s for $d_{b1} < d_{b2}$ and $d_{b1} = d_{b2}$. In the first case, the two peaks are close due to the fast crossing of the deeper and thinner layer; in the second case, a larger temporal shifting between the two peaks is shown due to a longer time for crossing the deeper layer. On the contrary, when the upper hyporheic layer is characterized by a higher hydraulic conductivity, the *pdf*s are characterized by a single peak and a mild slope of their tails. In the three-layer system (see Figures 7d and 7e), we observe a narrower *pdf* with a single peak due to the confinement effect generated by the presence of the low permeability layer.

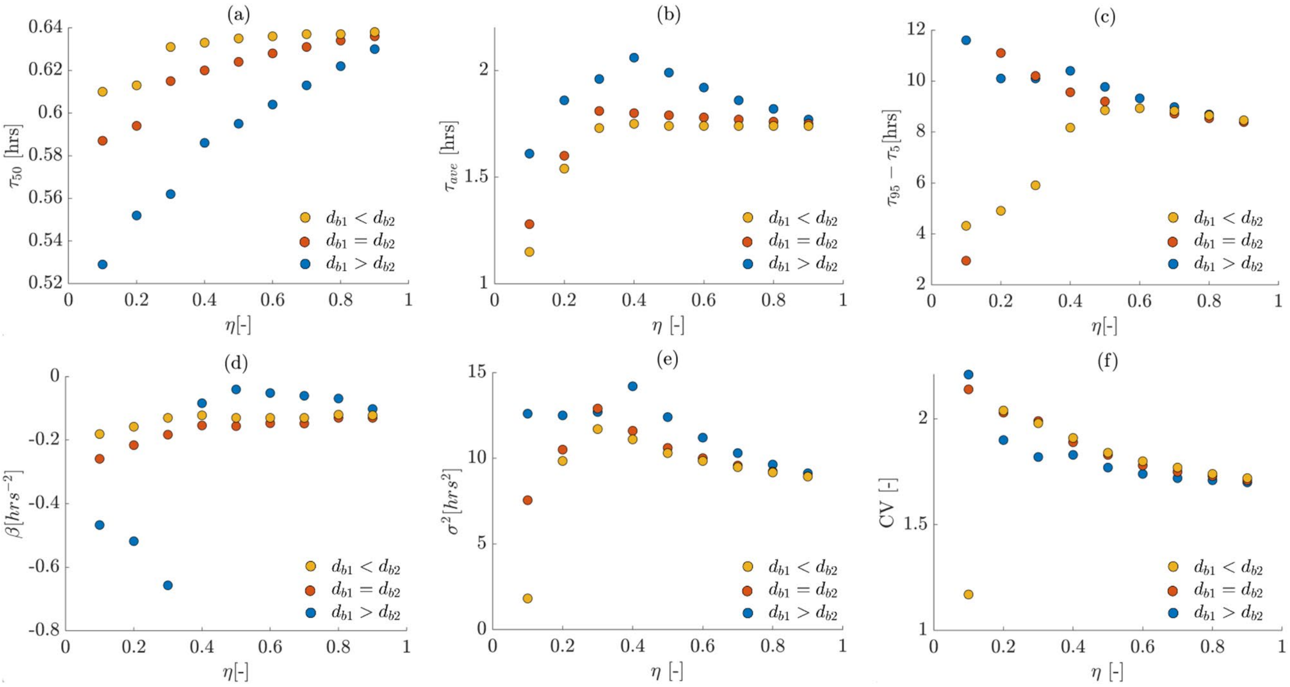

Figure 5. Variation of the statistical parameters characterizing the residence time distribution: (a) median hyporheic residence time, τ_{50}, (b) mean hyporheic residence time, τ_{ave}, (c) difference between the 95th and the 5th percentiles, (d) slope of the descending branch, β, (e) variance, σ^2, and (f) coefficient of variation, CV, as a function of $\eta = K_2/K_1$, for a three-layer system where a lower permeability strata (depth $d_l = 0.05$ m and hydraulic conductivity K_2) is located between: (a) d_{b1}(=0.05 m) < d_{b2}(=0.15 m) (yellow points), $d_{b1} = d_{b2}$(=0.10 m) (red points), and d_{b1}(=0.15 m) > d_{b2}(=0.05 m) (blue points).

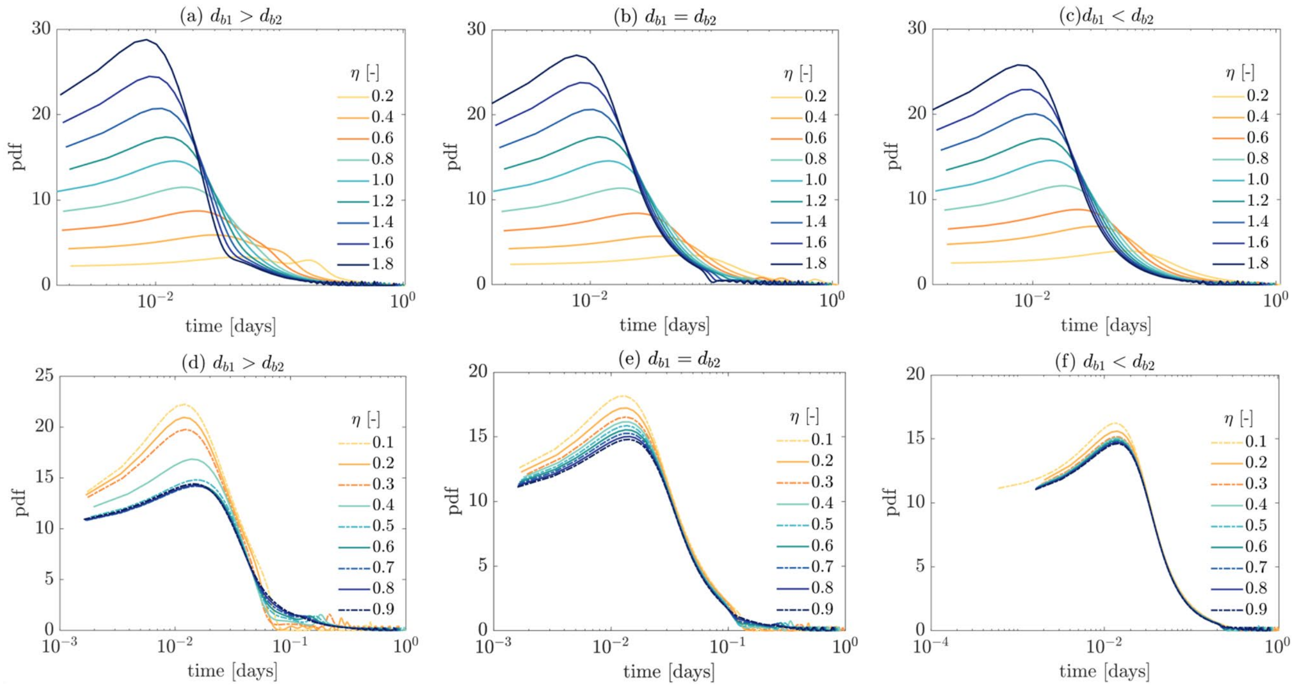

Figure 6. Residence time distribution (RTD) for different layered structures. The top row reports the two-layer configuration with: (a) $d_{b1} > d_{b2}$, (b) $d_{b1} = d_{b2}$, and (c) $d_{b1} < d_{b2}$. The bottom row reports the three-layer structure with a low permeability layer (depth $d_l = 0.05$ m and hydraulic conductivity K_2) located between: (a) $d_{b1} > d_{b2}$, (b) $d_{b1} = d_{b2}$, and (c) $d_{b1} < d_{b2}$. In each panel, different values of η are considered.

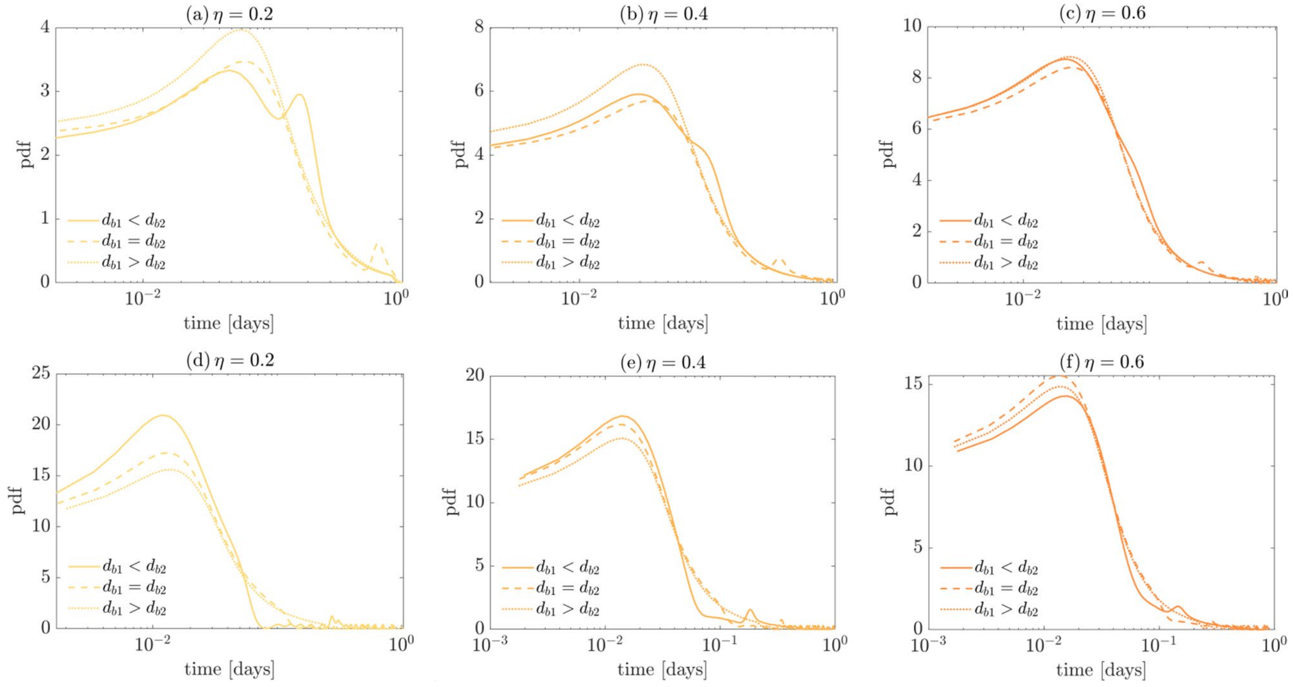

Figure 7. Residence time distribution (RTD) for different values of η: Panels (a, d) correspond to $\eta = 0.2$, panels (b, e) correspond to $\eta = 0.4$ and panels (c, f) are associated with $\eta = 0.6$. The hyporheic sediment is composed of a two-layered structure (top row) and a three-layered structure (bottom row).

Based on these results, we identify two statistics of the residence time as the most representative of the effect of the stratified structure of the streambed. Specifically, we select $\tau_{95} - \tau_5$ as a measure of dispersion and β as a measure of the importance of tailing-effects in the RTD for further analysis reported in the next section.

5. Model Reduction

This section explores the behavior of $\tau_{95} - \tau_5$ and β in the space of variability of selected parameters that embed the stratified structure of the streambed. To achieve this, we employ ROMs based on the PCE technique (Ghanem & Spanos, 1991; Xiu & Karniadakis, 2002) that provide an approximation of the response surface of the two quantities of interest in a computationally efficient way (e.g., Ciriello et al., 2017; Focaccia et al., 2021). This is useful to fully characterize how the layered formation and its features impact the RTD.

The general PCE framework is discussed in Appendix B. Here, we apply this framework to reconstruct the response of $\tau_{95} - \tau_5$ and β, for a two-layer structure, in the space of variability of the four parameters defining the logistic-type function in Equation 7, that is, the groundwater hydraulic conductivity K_g; the amplification/reduction factor $n = \alpha/K_g$ of the conductivity profile with respect to K_g; γ_t which reflects the location of the intersection of the two layers; k_r which measures the smoothness of the transition between the layers. For a well-sorted sand type of soil, plausible ranges of values for these parameters are identified and translated into uniform distributions to provide a probabilistic representation of their variability (see Table 1).

Table 1
Distributions of Selected Parameters for the Application of the ROM

Parameter	Distribution
K_g (m/d $\times 10^{-2}$)	$\mathcal{U}[0.25; 0.9]$
n $(-)$	$\mathcal{U}[0.5; 1.5]$
k_r $(-)$	$\mathcal{U}[-0.1; 0.1]$
γ_t $(-)$	$\mathcal{U}[0.1; 0.9]$

Note. Parameters are distributed according to the uniform distribution, denoted by $\mathcal{U}[\pi_o, \pi_f]$, where π_o and π_f are the lower and upper bounds of the distribution.

As a consequence, the PCE approximations of $\tau_{95} - \tau_5$ and β read as follows:

$$(\tau_{95} - \tau_5) \approx \sum_{i=0}^{P-1} a_i(\mathbf{k})\Psi_i(\mathbf{p}), \tag{28}$$

$$\beta \approx \sum_{i=0}^{P-1} b_i(\mathbf{k})\Psi_i(\mathbf{p}), \tag{29}$$

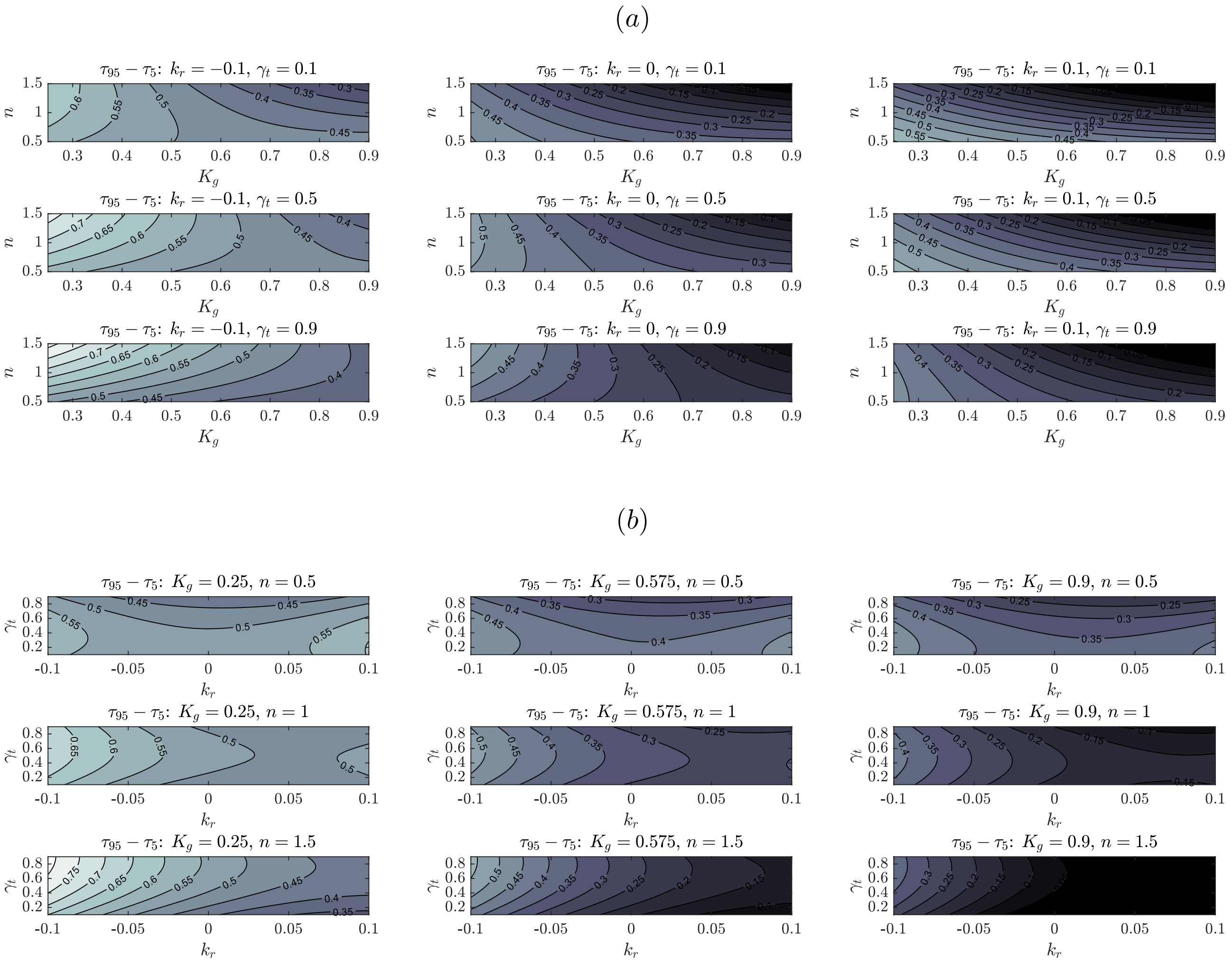

Figure 8. Approximated response surfaces of $\tau_{95} - \tau_5$ (in days) in the space (a) $K_g - n$ for different values of k_r and γ_t, and (b) $k_r - \gamma_t$ for different values of K_g (in m/d × 10^{-2}) and n.

where $M = \dim(\mathbf{p}) = 4$, $\mathbf{p} = (p_1, p_2, p_3, p_4)$. In this example, p_1, p_2, p_3, p_4 are linked to K_g, n, k_r, γ_t via an isoprobabilistic transform (e.g., Sudret, 2008); we use a second-order expansion, that is, $q = 2$, so that the number of terms in Equations 28 and 29 is $P = 15$. This also represents the number of regression points needed to compute the PCE coefficients, a_i and b_i, that is, the number of times we have to run the physically based model proposed in this study to train the PCE-based ROMs. Polynomials Ψ_i belong to the family of the Legendre polynomials that represents an orthonormal basis with respect to a uniform probability measure (e.g., Xiu & Karniadakis, 2002).

Note that coefficients a_i and b_i incorporate the dependence on single point values associated with deterministic parameters that concur to define the scenario selected for this analysis. The selected scenario is based on data from experiment number 4 in Marion et al. (2008) assuming negligible the channel slope and a neutral groundwater conditions (i.e., $s = 0$, $q_{gw} = 0$). In order to delineate all the possible flow pathlines that characterize the hyporheic flow, we assume $d_b = L = 0.5$ m. Other relevant parameters are: $Y_0 = 0.15$ m, $Q = 0.009$ m^3/s, $V = 0.36$ m/s, and $H_d = 0.05$ m.

The validation of the ROMs and the statistical characterization of the quantities of interest as a consequence of the parameter variability are discussed in Appendix B. Once the ROMs are available, we easily reconstruct the response surfaces of the two quantities of interest in the space of two parameters at a time, while varying the other two. Specifically, Figures 8a and 8b provide the response surface of $\tau_{95} - \tau_5$ in (a) the space $K_g - n$ for different values of k_r and γ_t, and (b) in the space $k_r - \gamma_t$ for different values of K_g and n, respectively. A similar analysis for β is carried out in Figures 9a and 9b. We generally observe that $\tau_{95} - \tau_5$ is mainly sensitive to variations in

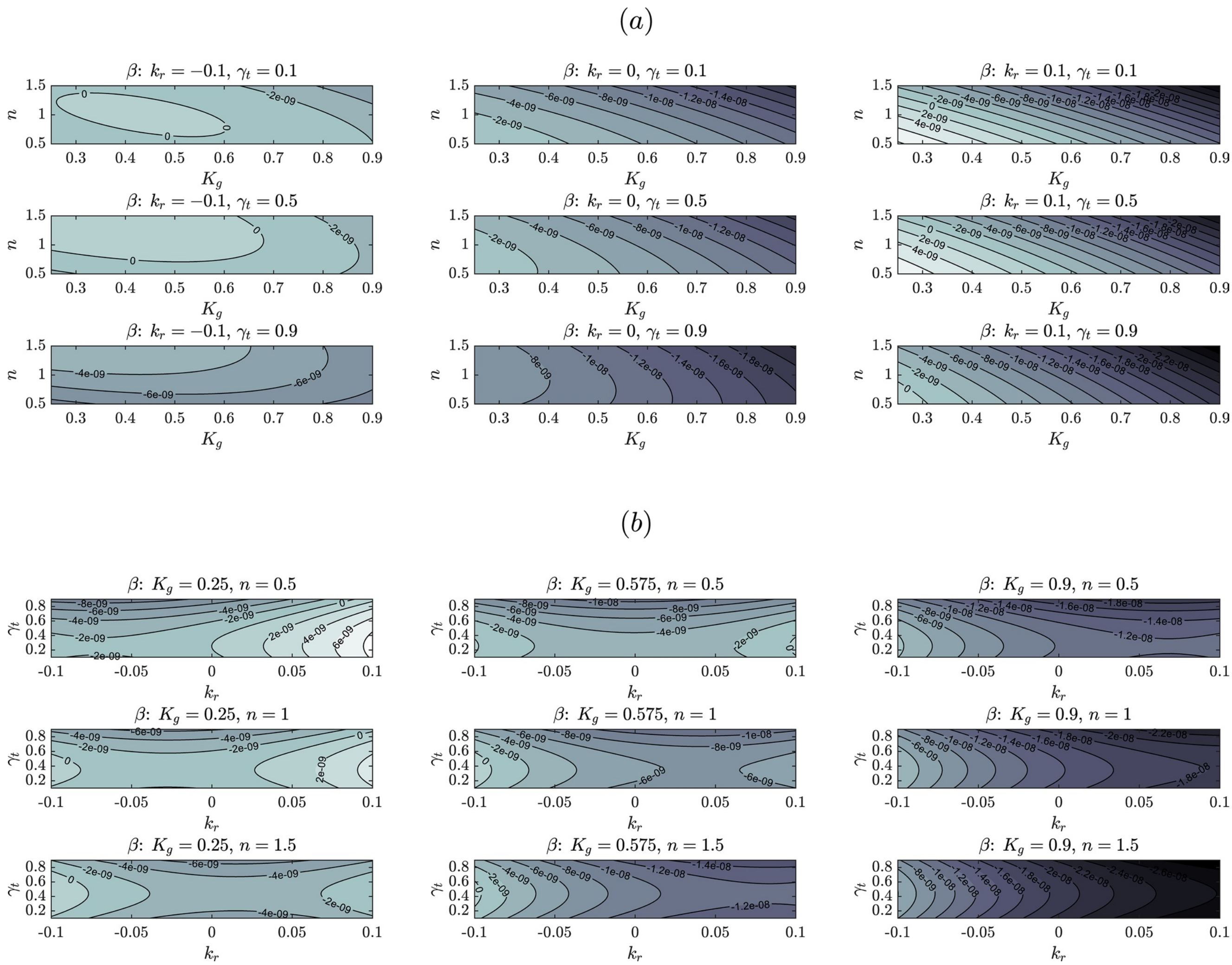

Figure 9. Approximated response surfaces of β in the space (a) $K_g - n$ for different values of k_r and γ_t, and (b) $k_r - \gamma_t$ for different values of K_g (in m/d × 10^{-2}) and n.

K_g (Figure 8a) and k_r (Figure 8b). The same holds when observing Figures 9a and 9b (related to β). A secondary role is played by n in both cases. Note that, in the selected logistic-type function for the conductivity field (Equation 7), K_g reflects the minimum value assumed by the hydraulic conductivity along the vertical profile.

As shown in Figure 8a, the difference between the travel time percentiles is reduced by more than half when increasing K_g in its range of variability. This effect is further emphasized when the value of k_r increases, that is, when the hydraulic conductivity decreases with depth. In general, the higher k_r, the lower $\tau_{95} - \tau_5$ (Figure 8b). Overlapped to this main behavior, there is the influence played by n; its secondary role can be appreciated, in particular, in two cases: for high γ_t when $k_r < 0$ and for low values of γ_t when $k_r > 0$, being γ_t the depth of the inflection point of the profile. The first is the case in which we have lower hydraulic conductivity on top, but it increases quickly with depth; while, in the second case, the hydraulic conductivity preserves high values for almost the entire vertical profile. In the first case, the difference between the quantiles increases with n, while the opposite is in the second case. As for β, it decreases when K_g increases and the more rapidly the higher k_r is. With a secondary effect, it also decreases with increasing n and γ_t as shown in Figures 9a and 9b.

6. Summary

Streambed sediments are ubiquitously heterogeneous. The variability of the hydraulic conductivity impacts solute residence times as well as mass fluxes which have a clear impact on hyporheic ecosystems. In our study, we derived an integral transform-based solution for the hyporheic flow in the presence of conductivity heterogeneity. Heterogeneity is conceptualized in the form of stratification, that is, the hydraulic conductivity varies vertically. Based on the observed data, we propose the use of a logistic-type function that is flexible to mimic the fluctuations of hydraulic conductivity with depth. By mathematically representing the heterogeneous hyporheic zone through a single domain formulation, the derived solution naturally the continuity conditions, for example, prescribed heads and fluxes, at the interface of each stratum. Aside from the computational advantages associated with the analytical features of the solution methodology, the integral transform-based solution (together with particle tracking) is (a) capable of reproducing data from multiple experimental tracer tests and (b) successfully compared to the results from a numerical simulator.

We apply our modeling framework to investigate the impact of sediment heterogeneity on key statistics and distribution of the solute residence time. In particular, we quantify the effect of the hydraulic conductivity contrasts in a two-layer system and identify the most affected statistics of the solute travel time: (a) the inter-percentile difference $\tau_{95} - \tau_5$ which represents a measure of dispersion, and (b) the slope β of the descending branch of the RTD as a measure of the importance of tailing-effects. For these two quantities of interest, we employ ROMs to explore their behavior in the space of variability of the parameters used in the logistic-type function (reflecting the hydraulic conductivity variability), to fully characterize how the layered formation and its features impact the RTD, at a negligible computational cost.

Although the results are limited to steady-state flows and the boundary conditions adopted, the integral transform method can be employed to address more complex scenarios. If different boundary conditions are used, one needs to modify boundary conditions in the Sturm-Liouville problem, see Equation 13. This modification will lead to different eigenfunctions and eigenvalues. To incorporate transient effects on the hydraulic head, the solution strategy would consist simply of performing the integral transformation in the spatial dimensions, namely x and z. Such transformation would yield a system of coupled first-order ordinary differential equations (in time) which can be solved numerically. The solution of the system of coupled ordinary differential equations would then be used in the inverse formula to obtain a series expansion of the hydraulic head in space and in time.

The proposed methodology and the obtained results are extremely relevant as hyporheic exchange affects multiple freshwater and groundwater processes. The semi-analytical solution allows us to better understand the impact of permeability structure on flow and transport. Moreover, the proposed reduced order model is a computationally efficient tool that allows one to perform global sensitivity analysis and uncertainty quantification. To our knowledge, this is the first time such tools are employed to investigate flow and transport in the hyporheic zone. The analysis of the effects of hydraulic conductivity on the *pdf* of the RTD helps in understanding how solutes and contaminants move between surficial and sub-surficial environments as well as to characterize the fate of some chemicals and water quality parameters (i.e., dissolved oxygen and temperature) that can affect the presence and distribution of microorganisms at the water-sediment interface.

Appendix A: Comparison With Numerical and Experimental Data

A1. Numerical Data

The proposed semi-analytical solution for the hydraulic head, Equation 10, is compared with numerical simulations obtained with the Python package FloPy (Bakker et al., 2016), which is based on the finite-difference solver for the groundwater flow equation, MODFLOW (Harbaugh, 2005). For this comparison, we consider two cases: the flow through a homogeneous streambed (Figure A1a), with hydraulic conductivity $K = 5 \times 10^{-5}$m/s, and flow through a heterogeneous streambed (Figure A1b), with hydraulic conductivity changing with depth and mimicking a four layer strata with K ranging between 5×10^{-4}m/s and 5×10^{-3}m/s. For the homogeneous case, Figure A1a also depicts the comparison with the fully analytical solution proposed in the past (Marzadri et al., 2016) (asterisk filled points). In both cases the domain size is $L = 3$ m and $d_b = 3$ m. Other parameters used in the simulations are: $V = 0.252$ m/s, $H_d = 0.06$ m, $Y_0 = 0.177$ m, $s = 0$ and $q_g = 0$ (i.e., streambed of negligible slope and absence of groundwater flow).

Figure A1 shows the excellent agreement between the values of hydraulic head predicted by the semi-analytical solution and the numerical model at different depths in the hyporheic zone and for different heterogeneous conditions. Furthermore, it emphasizes how the solution is capable of recovering the fully analytical solution reported in the literature (Marzadri et al., 2016).

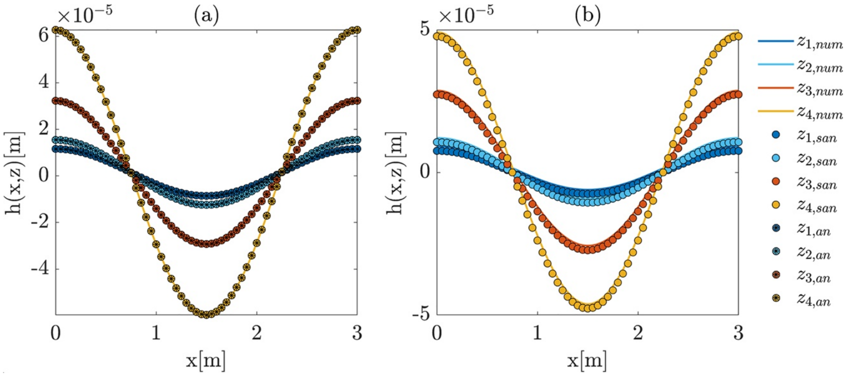

Figure A1. Comparison between predictions of hydraulic head, $h(x, z)$, obtained through the proposed semi-analytical solution (points identified with subscript "*san*") and numerical simulations lines identified with subscript "*num*") at different depths, $z_1 = 0.25$ m, $z_2 = 0.50$ m, $z_3 = 1$ m, and $z_4 = 1.5$ m, within the hyporheic zone. Panel (a) shows the comparison of the semi-analytical solution for an homogeneous streambed sediment with the analytical solution provided by Marzadri et al. (2016) (asterisk filled points identified with subscript "*an*") and the fully numerical solution. Panel (b) shows the comparison between the semi-analytical and the numerical solutions for a stratified streambed sediment composed by four layers with different hydraulic conductivity.

A2. Experimental Data

Next, we compare transport predictions provided by our modeling framework with experimental results reported by Marion et al. (2008) that consist of the penetrated mass of a passive tracer in flume experiments. To this end, we set $H_d = 0.05$ m and $L = 0.5$ m, while other hydraulic characteristics of the stream water are reported in Marion et al. (2008), see their experimental set-up numbers 4 and 6 in Table 1. Accordingly, we simulate a two-layer hyporheic sediment with a total depth of $d_b = 0.15$ m. In this two-layer system, a low hydraulic conductivity medium, $K_1 = 3 \times 10^{-4}$ m/s $= 25.92$ m/d, is located at the bottom of the hyporheic zone with thickness $d_{b1} = 0.12$ m. To generate this stratification in Equation 7, we used the following parameters: $K_g = 5 \times 10^{-4}$m/s, $N_k = 1$, $\alpha = 0.02$, $\gamma_t = 0.8$, and $k_r = 0.02$. The upper soil layer has a higher hydraulic conductivity, $K_2 = 0.02$ m/s $= 1{,}728$ m/d, and thickness $d_{b2} = 0.03$ m.

The statistical interpretation of the residence times allows to evaluate the cumulative mass exchange (per unit streambed area) between the stream and the surrounding hyporheic zone according to Equation 27. In this equation, $m(t)$ is a length representing the mass flux entering and accumulating within the hyporheic zone. Consequently, in the representation of the results, we use a dimensionless mass obtained by normalizing $m(t)$ by the ratio $\phi/(2\pi)^2$ of the dune wavelength (Elliott & Brooks, 1997).

As depicted in Figure A2, the dimensionless mass provided by the proposed model is able to capture the dynamic behavior of experimental measures for both the hydro-morphological characteristics of the two experiments. When compared to the model provided by Marion et al. (2008), the proposed model is able to capture the dimensionless mass along faster pathlines connecting downwelling-upwelling areas (especially in Figure A2a), thus underlining its capability as a predictive tool for investigating hyporheic exchange in layered alluvial sediments.

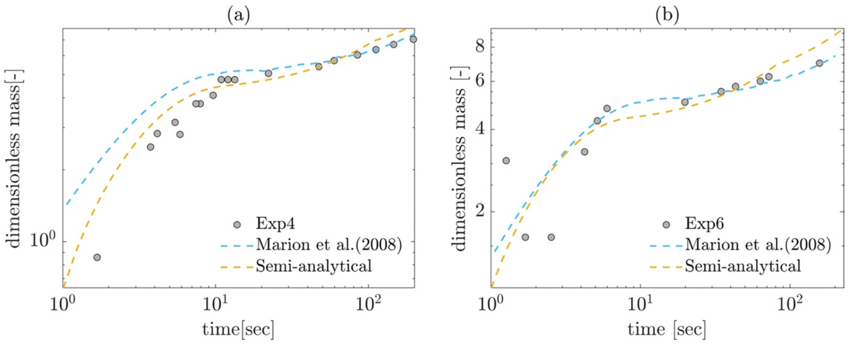

Figure A2. Comparison between predictions of dimensionless solute mass penetrated within the hyporheic zone as a function of time for the hydro-morphological characteristics of experiments 4 (left panel) and 6 (right panel) in Marion et al. (2008). Gray dots represent the experimental measures, while light-blue and light-orange dashed lines represent predictions provided by the model in Marion et al. (2008) and by the proposed modeling framework, respectively.

Appendix B: Theory and Validation of the ROMs

B1. PCE Framework

Let ω be a generic quantity of interest provided by a physically based model (e.g., a governing equation). The PCE approximation of ω reads as follows:

$$\hat{\omega} = \sum_{i=0}^{P-1} s_i \Psi_i(\mathbf{p}), \qquad P = \frac{(M+q)!}{M!q!}, \tag{B1}$$

where $\mathbf{p}$ is the vector of governing parameters, modeled as independent random variables, $M = \dim(\mathbf{p})$, Ψ_i are multivariate polynomials which constitute an orthonormal basis with respect to the joint *pdf* of $\mathbf{p}$, q is the maximum degree of the expansion, and coefficients s_i are the deterministic coordinates of the spectral decomposition (e.g., Sudret, 2008; Xiu & Karniadakis, 2002). A regression-based approach is employed to compute the unknown coefficients s_i; it consists in the minimization of the variance of a residual defined as the difference between ω and $\hat{\omega}$ at an optimal set of regression points in the (random) parameter space as provided by the probabilistic collocation method (e.g., Sudret, 2008).

B2. Validation and Statistical Characterization

Figures B1a–B1c depict the approximated *pdf* of $\tau_{95} - \tau_5$ computed by performing a Monte Carlo simulation on Equation 28 and the validation of the ROM at 110 points randomly selected in the parameter space, respectively. The total number of realizations used for the Monte Carlo simulation is $N_{sim} = 50{,}000$. Similar analysis is carried out for β, Equation 29, as displayed in Figures B1b–B1d.

The *pdf* of $\tau_{95} - \tau_5$ is characterized by a mean equal to 3.02×10^4 s, with a coefficient of variation of 0.37. The *pdf* of β is characterized by a mean equal to -6.56×10^{-9}, with a coefficient of variation of 0.79. These values suggest the relevance of analyzing the impact of the variability of the parameters characterizing the stratified structure of the streambed on both the quantities of interest. We note, that the accuracy of the PCE ROMs is remarkable when compared to the physically based high fidelity model. We obtain $R^2 = 0.74$ and the slope of the regression line equal to 0.94 for $\tau_{95} - \tau_5$. We have $R^2 = 0.78$ and the slope of the regression line equal to 1.10 for β.

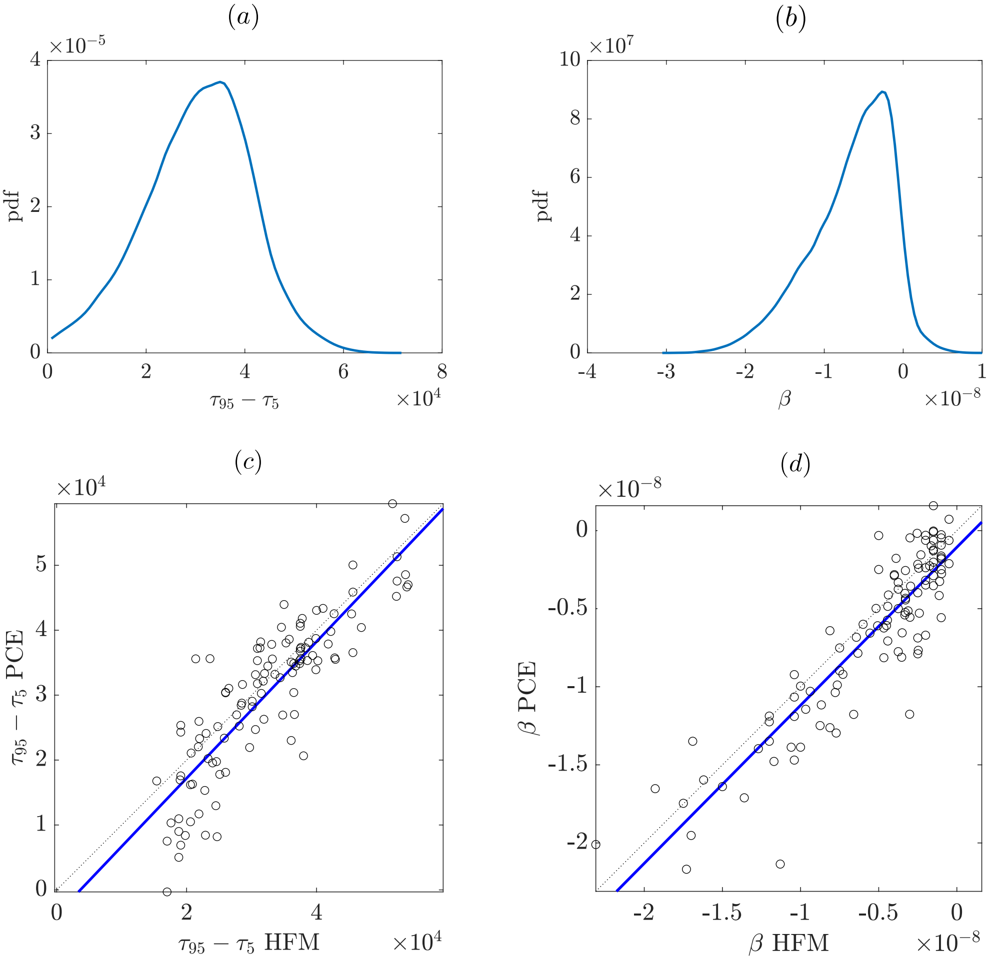

Figure B1. (a, b) Depict the approximated *pdfs* of $\tau_{95} - \tau_5$ (in s) and β respectively computed with the PCE ROMs; (c, d) show the comparison between predictions of the two quantities of interest as provided by the physically based high-fidelity model (HFM) and the second-order PCEs at 110 points in the random parameter space; the regression line (in blue) and the bisector (dashed black line) are also represented.

Appendix C: Hyporheic Flow Field in a Two-Layer System

Figure C1 integrates the results presented in Figure 5 by analyzing a hyporheic zone represented by a two-layer structure (as sketched in Figure 3). Here, K_1 is kept constant and equal to 110 m/d; while K_2 is varied between 22 m/d and 198 m/d (i.e., $\eta = 0.2 \div 1.8$). This variability range is chosen in order to explore how the range of hydraulic conductivities observed in sandy rivers (Walker et al., 2018) could potentially impact the main parameters affecting the RTD.

In Figure C1a, we observe that τ_{50} decreases as η increases, for the different configurations of layer depths. The results illustrate that the hydraulic conductivity near the water-sediment interface favors fast transport across the hyporheic zone. Indeed, for $\eta \geq 1$, the effect of the layer depth on τ_{50} is negligible, while for low values of η, the highest values of τ_{50} occur for the case $d_{b1} < d_{b2}$. Also τ_{ave} decreases as η increases (Figure C1b). We note that for $\eta > 1$, τ_{ave} is slightly higher for $d_{b1} < d_{b2}$; while the highest values occur for $d_{b1} = d_{b2}$ in case $\eta < 1$, when the entrance of particles (and the flow) within the hyporheic zone is slow. The effects of the stratification become more evident for $\tau_{95} - \tau_5$, β, and σ^2 (Figures C1c–C1e, respectively). In Figures C1c and C1e, we observe that the values of the statistical parameters decrease as η increases. However, the variability of values assumed by both $\tau_{95} - \tau_5$ and σ^2 is higher, especially for low η, indicating that the different scenarios of stratification impact more the dispersion of residence time values. Specifically, the highest dispersion is noted in case of $\eta < 0.5$ and $d_{b1} = d_{b2}$. As for β, the decrease for increasing η is faster when $\eta > 1$, except if $d_{b1} > d_{b2}$; in this case the decrease

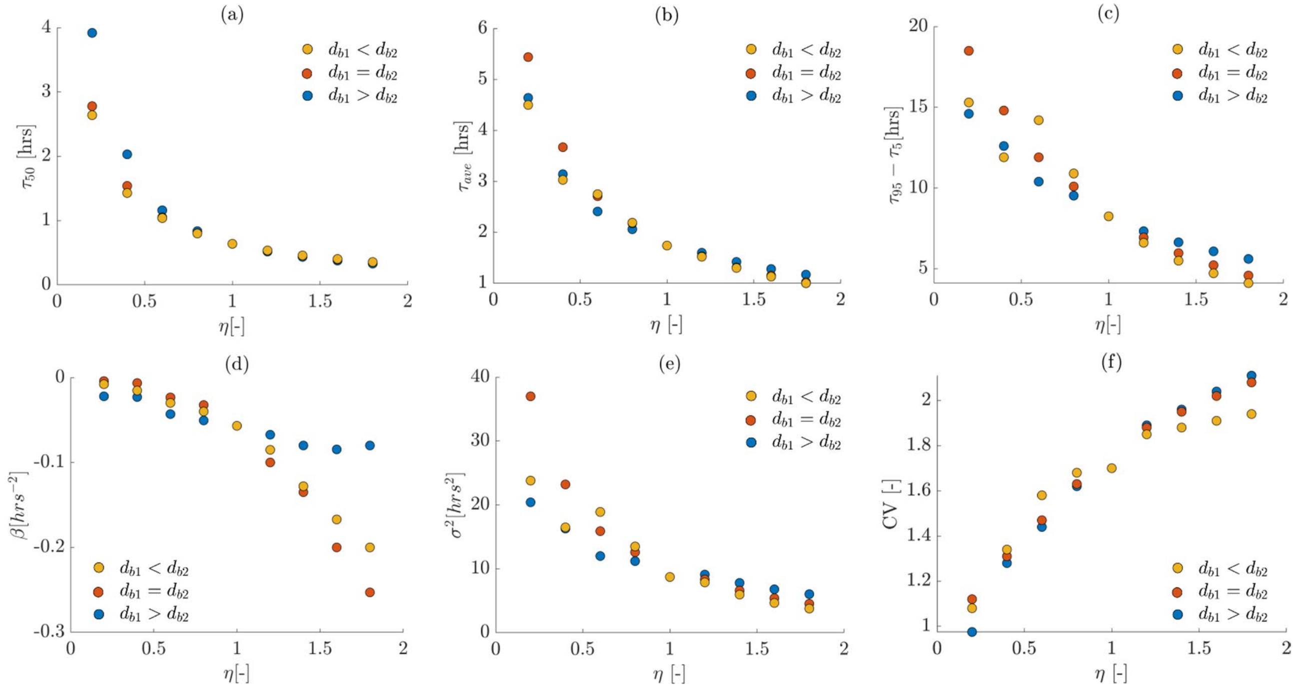

Figure C1. Variation of statistical parameters of the residence time distribution: (a) median hyporheic residence time, τ_{50}, (b) mean hyporheic residence time, τ_{ave}, (c) difference between the 95th and the 5th percentiles, (d) slope of the descending branch, β, (e) variance, σ^2, and (f) coefficient of variation, CV, as a function of $\eta = K_2/K_1$, for different layered structures: d_{b1}(=0.05 m) < d_{b2}(=0.20 m) (yellow points), $d_{b1} = d_{b2}$(=0.125 m) (red points), and d_{b1}(=0.20 m) > d_{b2}(=0.05 m) (blue points).

of β is smooth and smaller in the value. Finally, Figure C1f shows that CV increases with η as a combination of the decreasing of both σ^2 and τ_{ave}, with a shift in the highest values between $d_{b1} < d_{b2}$ when $\eta < 1$ and vice versa. This behavior occurs because the stratification characteristics of the hyporheic layers influence the tails of the *pdf* and consequently the statistical dispersion of data around the mean (see also Figures 6 and 7).

Data Availability Statement

All the relevant information necessary for reproducing the results from this paper can be found in the text. There are no data-sharing issues since all of the numerical results are provided in the figures produced by solving the governing equations provided in the paper.

Acknowledgments
The authors acknowledge the constructive comments raised by all reviewers and the Editors. A.M. acknowledges funding from the Italian Ministry of Education, University and Research (MIUR) in the framework of the Departments of Excellence Initiative 2023-2027. This study was carried out also within the PNRR research activities of the consortium iNEST (Interconnected NorthEst Innovation Ecosystem) funded by the European Union NextGenerationEU (Piano Nazionale di Ripresa e Resilienza (PNRR) - Missione 4 Componente 2, Investimento 1.5 - D.D. 1058 23/06/2022, ECS 00000043). The last author acknowledges the support from NSF Grant 1654009. This article reflects only the author's views and opinions.

References

Bakker, M., Post, V., Langevin, C. D., Hughes, J. D., White, J. T., Starn, J. J., & Fienen, M. N. (2016). Scripting MODFLOW model development using Python and FloPy. *Groundwater*, *54*(5), 733–739. https://doi.org/10.1111/gwat.12413

Barbuto, F. A. A., & Cotta, R. M. (1997). Integral transformation of elliptic problems within irregular domains: Fully developed channel flow. *International Journal of Numerical Methods for Heat and Fluid Flow*, *7*(8), 778–793. https://doi.org/10.1108/09615539710193065

Bencala, K., & Walters, R. (1983). Simulation of solute transport in a mountain pool-and-riffle stream: A transient storage model. *Water Resources Research*, *19*(3), 718–724. https://doi.org/10.1029/WR019i003p00718

Boano, F., Demaria, A., Revelli, R., & Ridolfi, L. (2010). Biogeochemical zonation due to intrameander hyporheic flow. *Water Resources Research*, *46*(2), W02511. https://doi.org/10.1029/2008WR007583

Boano, F., Revelli, R., & Ridolfi, L. (2008). Reduction of the hyporheic zone volume due to the stream-aquifer interaction. *Geophysical Research Letters*, *35*(9), L09401. https://doi.org/10.1029/2008gl033554

Bonazzi, A., Jha, B., & de Barros, F. P. J. (2021). Transport analysis in deformable porous media through integral transforms. *International Journal for Numerical and Analytical Methods in Geomechanics*, *45*(3), 307–324. https://doi.org/10.1002/nag.3150

Buffington, J. M., & Montgomery, D. R. (1999). A procedure for classifying textural facies in gravel-bed rivers. *Water Resources Research*, *35*(6), 1903–1914. https://doi.org/10.1029/1999WR900041

Cardenas, M., Wilson, J., & Haggerty, R. (2008). Residence time of bedform-driven hyporheic exchange. *Advances in Water Resources*, *31*(10), 1382–1386. https://doi.org/10.1016/j.advwatres.2008.07.006

Cardenas, M., Wilson, J. L., & Zlotnik, V. A. (2004). Impact of heterogeneity, bed forms, and stream curvature on subchannel hyporheic exchange. *Water Resources Research*, *40*(8), W08307. https://doi.org/10.1029/2004wr003008

Ciriello, V., & de Barros, F. P. J. (2020). Characterizing the influence of multiple uncertainties on predictions of contaminant discharge in groundwater within a Lagrangian stochastic formulation. *Water Resources Research*, *56*(10), e2020WR027867. https://doi.org/10.1029/2020wr027867

Ciriello, V., Lauriola, I., Bonvicini, S., Cozzani, V., Di Federico, V., & Tartakovsky, D. M. (2017). Impact of hydrogeological uncertainty on estimation of environmental risks posed by hydrocarbon transportation networks. *Water Resources Research*, *53*(11), 8686–8697. https://doi.org/10.1002/2017WR021368

Ciriello, V., Lauriola, I., & Tartakovsky, D. M. (2019). Distribution-based global sensitivity analysis in hydrology. *Water Resources Research*, *55*(11), 8708–8720. https://doi.org/10.1029/2019wr025844

Cisneros, J., Best, J., van Dijk, T., Almeida, R. P. D., Amsler, M., Boldt, J., et al. (2020). Dunes in the world's big rivers are characterized by low-angle lee-side slopes and a complex shape. *Nature Geoscience*, *13*(2), 156–162. https://doi.org/10.1038/s41561-019-0511-7

Cotta, R. M. (1993). *Integral transforms in computational heat and fluid flow*. CRC Press.

Cotta, R. M., Lisboa, K. M., & Zotin, J. L. Z. (2020). Integral transforms for flow and transport in discrete and continuum models of fractured heterogeneous porous media. *Advances in Water Resources*, *142*, 103621. https://doi.org/10.1016/j.advwatres.2020.103621

Dagan, G., Cvetkovic, V., & Shapiro, A. (1992). A solute flux approach to transport in heterogeneous formations: 1. The general framework. *Water Resources Research*, *28*(5), 1369–1376. https://doi.org/10.1029/91WR03086

de Barros, F. P. J., & Cotta, R. M. (2007). Integral transforms for three-dimensional steady turbulent dispersion in rivers and channels. *Applied Mathematical Modelling*, *31*(12), 2719–2732. https://doi.org/10.1016/j.apm.2006.10.024

de Barros, F. P. J., Mills, W. B., & Cotta, R. M. (2006). Integral transform solution of a two-dimensional model for contaminant dispersion in rivers and channels with spatially variable coefficients. *Environmental Modelling & Software*, *21*(5), 699–709. https://doi.org/10.1016/j.envsoft.2005.02.002

Elliott, A. H., & Brooks, N. H. (1997). Transfer of nonsorbing solutes to a streambed with bed forms: Theory. *Water Resources Research*, *33*(1), 123–136. https://doi.org/10.1029/96wr02784

Findlay, S. (1995). Importance of surface-subsurface exchange in stream ecosystems: The hyporheic zone. *Limnology & Oceanography*, *40*(1), 159–164. https://doi.org/10.4319/lo.1995.40.1.0159

Focaccia, S., Panini, G., Pedrazzoli, P., & Ciriello, V. (2021). A meta-modeling approach for hydrological forecasting under uncertainty: Application to groundwater nitrate response to climate change. *Journal of Hydrology*, *603*, 127173. https://doi.org/10.1016/j.jhydrol.2021.127173

Fox, A., Laube, G., Schmidt, C., Fleckenstein, J., & Arnon, S. (2016). The effect of losing and gaining flow conditions on hyporheic exchange in heterogeneous streambeds. *Water Resources Research*, *52*(9), 7460–7477. https://doi.org/10.1002/2016wr018677

Frei, S., Azizian, M., Grant, S. B., Zlotnik, V. A., & Toundykov, D. (2019). Analytical modeling of hyporheic flow for in-stream bedforms: Perturbation method and implementation. *Environmental Modelling & Software*, *111*, 375–385. https://doi.org/10.1016/j.envsoft.2018.09.015

Ghanem, R. G., & Spanos, P. D. (1991). *Stochastic finite element—A spectral approach*. Springer.

Harbaugh, A. W. (2005). MODFLOW-2005, the U.S. geological survey modular ground-water model—The ground-water flow process. *U.S. Geological Survey Techniques and Methods*, 6-A16.

Hester, E. T., Young, K. I., & Widdowson, M. A. (2013). Mixing of surface and groundwater induced by riverbed dunes: Implications for hyporheic zone definitions and pollutant reactions. *Water Resources Research*, *49*(9), 5221–5237. https://doi.org/10.1002/wrcr.20399

Jiang, Q., Jin, G., Tang, H., Shen, C., Cheraghi, M., Xu, J., et al. (2020). Density-dependent solute transport in a layered hyporheic zone. *Advances in Water Resources*, *142*, 103645. https://doi.org/10.1016/j.advwatres.2020.103645

Jury, W. A., Sposito, G., & White, R. E. (1986). A transfer function model of solute transport through soil: 1. Fundamental concepts. *Water Resources Research*, *22*(2), 243–247. https://doi.org/10.1029/WR022i002p00243

Knupp, D. C., Cotta, R. M., & Naveira-Cotta, C. P. (2015). Fluid flow and conjugated heat transfer in arbitrarily shaped channels via single domain formulation and integral transforms. *International Journal of Heat and Mass Transfer*, *82*, 479–489. https://doi.org/10.1016/j.ijheatmasstransfer.2014.11.007

Ling, B., Rizzo, C. B., Battiato, I., & de Barros, F. P. J. (2021). Macroscale transport in channel-matrix systems via integral transforms. *Physical Review Fluids*, *6*(4), 044501. https://doi.org/10.1103/physrevfluids.6.044501

Małoszewski, P., & Zuber, A. (1982). Determining the turnover time of groundwater systems with the aid of environmental tracers: 1. Models and their applicability. *Journal of Hydrology*, *57*(3), 207–231. https://doi.org/10.1016/0022-1694(82)90147-0

Marion, A., Packman, A. I., Zaramella, M., & Bottacin-Busolin, A. (2008). Hyporheic flows in stratified beds. *Water Resources Research*, *44*(9), W09433. https://doi.org/10.1029/2007wr006079

Marklund, L., & Wörman, A. (2011). The use of spectral analysis-based exact solutions to characterize topography-controlled groundwater flow. *Hydrogeology Journal*, *19*(8), 1531–1543. https://doi.org/10.1007/s10040-011-0768-4

Marzadri, A., Tonina, D., & Bellin, A. (2012). Morphodynamic controls on redox conditions and on nitrogen dynamics within the hyporheic zone: Application to gravel bed rivers with alternate-bar morphology. *Journal of Geophysical Research: Biogeosciences*, *117*(G3), G00N10. https://doi.org/10.1029/2012jg001966

Marzadri, A., Tonina, D., Bellin, A., & Valli, A. (2016). Mixing interfaces, fluxes, residence times and redox conditions of the hyporheic zones induced by dune-like bedforms and ambient groundwater flow. *Advances in Water Resources*, *88*, 139–151. https://doi.org/10.1016/j.advwatres.2015.12.014

Marzadri, A., Tonina, D., Bellin, A., Vignoli, G., & Tubino, M. (2010). Semianalytical analysis of hyporheic flow induced by alternate bars. *Water Resources Research*, *46*(7), W07531. https://doi.org/10.1029/2009WR008285

Mikhailov, M. D., & Ozisik, M. N. (1994). *Unified analysis and solutions of heat and mass diffusion*. Dover Publications.

Nelson, A. R., Sawyer, A. H., Gabor, R. S., Saup, C. M., Bryant, S. R., Harris, K. D., et al. (2019). Heterogeneity in hyporheic flow, pore water chemistry, and microbial community composition in an alpine streambed. *Journal of Geophysical Research: Biogeosciences*, *124*(11), 3465–3478. https://doi.org/10.1029/2019JG005226

Nikora, V., Sukhodulov, A., & Rowinski, P. (1997). Statistical sand wave dynamics in one-directional water flows. *Journal of Fluid Mechanics*, *351*, 17–39. https://doi.org/10.1017/s0022112097006708

Oladyshkin, S., de Barros, F. P. J., & Nowak, W. (2012). Global sensitivity analysis: A flexible and efficient framework with an example from stochastic hydrogeology. *Advances in Water Resources*, *37*, 10–22. https://doi.org/10.1016/j.advwatres.2011.11.001

Packman, A. I., Brooks, N. H., & Morgan, J. J. (2000). A physicochemical model for colloid exchange between a stream and a sand streambed with bed forms. *Water Resources Research*, *36*(8), 2351–2361. https://doi.org/10.1029/2000wr900059

Pollock, D. (2012). *User guide for MODPATH version 6—A particle-tracking model for MODFLOW*. U.S. Geological Survey. Book 6, Chapter A41, 59.

Rizzo, C. B., Nakano, A., & de Barros, F. P. J. (2019). Par2: Parallel random walk particle tracking method for solute transport in porous media. *Computer Physics Communications*, *239*, 265–271. https://doi.org/10.1016/j.cpc.2019.01.013

Rubol, S., Battiato, I., & de Barros, F. P. J. (2016). Vertical dispersion in vegetated shear flows. *Water Resources Research*, *52*(10), 8066–8080. https://doi.org/10.1002/2016wr018907

Ryan, R., & Boufadel, M. (2006). Influence of streambed hydraulic conductivity on solute exchange with the hyporheic zone. *Environmental Geology*, *51*(2), 203–210. https://doi.org/10.1007/s00254-006-0319-9

Salehin, M., Packman, A. I., & Paradis, M. (2004). Hyporheic exchange with heterogeneous streambeds: Laboratory experiments and modeling. *Water Resources Research*, *40*(11), W11504. https://doi.org/10.1029/2003wr002567

Savant, S. A., Reible, D. D., & Thibodeaux, L. J. (1987). Convective transport within stable river sediments. *Water Resources Research*, *23*(9), 1763–1768. https://doi.org/10.1029/WR023i009p01763

Sawyer, A. H., & Cardenas, M. B. (2009). Hyporheic flow and residence time distributions in heterogeneous cross-bedded sediment. *Water Resources Research*, *45*(8), W08406. https://doi.org/10.1029/2008WR007632

Shen, H. W., Fehlman, H. M., & Mendoza, C. (1990). Bed form resistances in open channel flows. *Journal of Hydraulic Engineering*, *116*(6), 799–815. https://doi.org/10.1061/(asce)0733-9429(1990)116:6(799)

Stonedahl, S. H., Harvey, J., Wörman, A., Salehin, M., & Packman, A. (2010). A multiscale model for integrating hyporheic exchange from ripples to meanders. *Water Resources Research*, *46*(12), W12539. https://doi.org/10.1029/2009wr008865

Stonedahl, S. H., Harvey, J. W., & Packman, A. I. (2013). Interactions between hyporheic flow produced by stream meanders, bars, and dunes. *Water Resources Research*, *49*(9), 5450–5461. https://doi.org/10.1002/wrcr.20400

Su, X., Yeh, T.-C. J., Shu, L., Li, K., Brusseau, M. L., Wang, W., et al. (2020). Scale issues and the effects of heterogeneity on the dune-induced hyporheic mixing. *Journal of Hydrology*, *590*, 125429. https://doi.org/10.1016/j.jhydrol.2020.125429

Sudret, B. (2008). Global sensitivity analysis using polynomial chaos expansions. *Reliability Engineering & System Safety*, *93*(7), 964–979. https://doi.org/10.1016/j.ress.2007.04.002

Tonina, D. (2012). Surface water and streambed sediment interaction: The hyporheic exchange. In C. Gualtieri & D. T. Mihailovic (Eds.), *Fluid mechanics of environmental interfaces* (2nd ed.). CRC Press, Taylor and Francis Group.

Tonina, D., & Buffington, J. M. (2007). Hyporheic exchange in gravel bed rivers with pool-riffle morphology: Laboratory experiments and three-dimensional modeling. *Water Resources Research*, *43*(1), W01421. https://doi.org/10.1029/2005WR004328

Tonina, D., de Barros, F. P. J., Marzadri, A., & Bellin, A. (2016). Does streambed heterogeneity matter for hyporheic residence time distribution in sand-bedded streams? *Advances in Water Resources*, *96*, 120–126. https://doi.org/10.1016/j.advwatres.2016.07.009

Tóth, J. (1963). A theoretical analysis of groundwater flow in small drainage basins. *Journal of Geophysical Research*, *68*(16), 4795–4812. https://doi.org/10.1029/jz068i016p04795

Trauth, N., Schmidt, C., Maier, U., Vieweg, M., & Fleckenstein, J. (2013). Coupled 3-D stream flow and hyporheic flow model under varying stream and ambient groundwater flow conditions in pool-riffle system. *Water Resources Research*, *49*(9), 5834–5850. https://doi.org/10.1002/wrcr.20442

Walker, D., Jovanovic, N., Bugan, R., Abiye, T., du Preez, D., Parkin, G., & Gowing, J. (2018). Alluvial aquifer characterisation and resource assessment of the Molototsi sand river, Limpopo, South Africa. *Journal of Hydrology: Regional Studies*, *19*, 177–192. https://doi.org/10.1016/j.ejrh.2018.09.002

Wörman, A., Packman, A. I., Marklund, L., Harvey, J. W., & Stonedahl, S. H. (2007). Fractal topography and subsurface water flows from fluvial bedforms to the continental shield. *Geophysical Research Letters*, *34*(7), L07402. https://doi.org/10.1029/2007gl029426

Xiu, D., & Karniadakis, G. E. (2002). The Wiener-Askey polynomial chaos for stochastic differential equations. *Journal of Scientific Computing*, *24*(2), 619–644. https://doi.org/10.1137/s1064827501387826

Zijl, W. (1999). Scale aspects of groundwater flow and transport systems. *Hydrogeology Journal*, *7*(1), 139–150. https://doi.org/10.1007/s100400050185